



HAL
open science

Development of an innovative heat exchanger for sensible heat storage in agro-food industry

M.A. Dekhil, J.V. Simo Tala, O. Bulliard-Sauret, D. Bougeard

► To cite this version:

M.A. Dekhil, J.V. Simo Tala, O. Bulliard-Sauret, D. Bougeard. Development of an innovative heat exchanger for sensible heat storage in agro-food industry. Applied Thermal Engineering, 2020, 177, 10.1016/j.applthermaleng.2020.115412 . hal-03224944

HAL Id: hal-03224944

<https://hal.science/hal-03224944>

Submitted on 22 Aug 2022

HAL is a multi-disciplinary open access archive for the deposit and dissemination of scientific research documents, whether they are published or not. The documents may come from teaching and research institutions in France or abroad, or from public or private research centers.

L'archive ouverte pluridisciplinaire **HAL**, est destinée au dépôt et à la diffusion de documents scientifiques de niveau recherche, publiés ou non, émanant des établissements d'enseignement et de recherche français ou étrangers, des laboratoires publics ou privés.



Distributed under a Creative Commons Attribution - NonCommercial 4.0 International License

1 Development of an innovative heat exchanger for sensible heat 2 storage in agro-food industry

3 **Mohamed Amine DEKHIL^{1,*}, Jules Voguelin SIMO TALA¹, Odin BULLIARD-
 4 SAURET^{1,2}, Daniel BOUGEARD¹**

5 ¹ IMT Lille Douai-941 Rue Charles Bourseul, 59500 Douai

6 ² HEI-Yncrea Hauts-de-France, 13 Rue de Toul, 59000 Lille

7 *(Corresponding author: mohamed-amine.dekhil@imt-lille-douai.fr; mohamed.amine.dekhil@
 8 gmail.com)

10 Abstract

11 The present article deals with the numerical study of the thermal behaviour of three
 12 configurations of heat exchangers for sensible thermal energy storage. The objective is to
 13 compare their response to transient thermal conditions in order to characterize their kinetics of
 14 charge/discharge of heat/cold. One of these heat exchangers is commonly encountered in agro-
 15 food industry and used in this study as the reference against which the other two configurations
 16 are compared. The reference heat exchanger is made up of two fluid coils embedded in an
 17 aluminium cylindrical conductive element. The other two heat exchangers are derived from this
 18 reference exchanger by a partial substitution of the conductive element with a confined heat
 19 transfer fluid. The compactness and heat exchange surfaces of the coils are identical in all three
 20 cases. The thermal behaviour and the storage performance of these heat exchangers are analysed
 21 using a three dimensional numerical study with the CFD code Star CCM + V12.02. This study
 22 shows that a controlled substitution of the conductive material by a confined heat transfer fluid,
 23 at constant compactness and coils heat transfer surface does not only achieve material saving
 24 compared to the reference configuration, but also increase the energy reserve without
 25 significant decrease in the heat transfer kinetics.

26 **Keywords:** Sensible Heat Storage, CFD, Thermal Analysis, Storage Performance, Transient
 27 state conditions, Charge/Discharge kinetics, Material saving.

28 Nomenclature

CFL	Courant number	-	T_{ref}	Reference temperature	K
C_p	Specific heat capacity	$J.kg^{-1}.K^{-1}$	\dot{T}_{cc}	Average kinetics of cooling during the charge	$K.s^{-1}$
$d_{coil, in}$	Inner diameter of the coil	m	\dot{T}_{cd}	Average kinetics of cooling during the discharge	$K.s^{-1}$
$d_{coil, out}$	Outer diameter of the coil	m	U_{max}	Maximum x-velocity	$m.s^{-1}$
E_{cdw}	Cooling energy discharged in confined water volumes	J	$U_{w, in}$	Water velocity at the inlet	$m.s^{-1}$
E_{csw}	Cooling energy stored by confined water volumes	J	V_{max}	Maximum y-velocity	$m.s^{-1}$
E_{tot}	Maximum energy stored	J	$V_{alu, sub}$	Total volume of substituted aluminium	m^3
f	Friction factor	-	V	Volume	m^3

g	Gravitational acceleration	$m.s^{-2}$	\vec{v}	Velocity vector	-
H	Heat exchanger height	m	X,Y,Z	Cartesian coordinates	-
P	Pressure	Pa	Greek symbols		
P_{coil}	Pitch of the coil	m	ρ	Density	$Kg.m^{-3}$
P_{vol}	Thermal power stored(during charge)/released(during discharge)	W	α	Thermal diffusivity	$m^2.s^{-1}$
$R_{curv,c}$	Radius of curvature of the cold coil	m	μ	Dynamic viscosity	Pa.s
$R_{curv,h}$	Radius of curvature of the hot coil	m	λ	Thermal conductivity	$W.m^{-1}.K^{-1}$
$R_{ex,in}$	Inner radius of the heat exchanger	m	β	Expansion coefficient	K^{-1}
$R_{ex,out}$	Outer radius of the heat exchanger	m	Abbreviations		
$r_{coil,in}$	Inner radius of the coil	m	al	Aluminium	
$r_{coil,out}$	Outer radius of the coil	m	cop	Copper	
R_{cc}	Cooling charge ratio	-	w	Water	
R_{cd}	Cooling discharge ratio	-	C2V	Configuration with two volumes of water	
Ra	Rayleigh number	-	C32V	Configuration with 32 volumes of water	
Re	Reynolds number	-	CFD	Computational fluid dynamics	
t	Time	s	HTF	Heat Transfer Fluid	
T	Temperature	K	HTIHE	High Thermal Inertia Heat Exchanger	
T_i	Initial temperature	K	LHTS	Latent Heat Thermal Storage	
$T_{in,c}$	Inlet temperature at the inlet of the cooling heat transfer fluid	K	SHTS	Sensible Heat Thermal Storage	
$T_{in,h}$	Inlet temperature at the inlet of the heating heat transfer fluid	K	TES	Thermal Energy Storage	

29
30

31 1. Introduction

32

33 Heat exchangers are thermodynamic equipment used in several industrial applications such as
34 automotive, chemical and process engineering, industrial heating, cooling and heat-recovery
35 processes, etc. [1-3]. In the most common applications, the heat transfer occurs under steady
36 state operating conditions. Priority is then given to steady state heat transfer which does not
37 allow any possibility of thermal energy storage in the heat exchanger. In some specific
38 applications such as thermal conditioning of beverage in agro-food industries, the heat
39 exchange between the heat transfer fluids occurs under transient state operation through a
40 conductive element which allows a better management of the heat or cold demand by storing
41 part of the thermal energy in the heat exchanger [4]. Thermal energy can be stored under
42 sensible [5-9], latent [10-13], or chemical [14-16] forms.

43 Among the above means of storing thermal energy, sensible heat thermal storage (SHTS) has
44 been drawing increasing attention. Technological and economical aspects make SHTS superior
45 to latent heat thermal storage (LHTS) [17]. It is the most common technology compared to other
46 storage methods [18], since it is by far the easiest to implement, simple in design and operation,
47 inexpensive and the most economical in a thermal energy storage (TES) system [19-20]. SHTS
48 consists in the heat stored by changing the temperature of a storage medium. The amount of
49 stored heat is proportional to the density, specific heat, volume, and temperature variation of

50 the storage materials. High energy density and good thermal conductivity are the most desirable
51 characteristics of sensible heat storage materials [21]. Other desirable characteristics are
52 good heat transfer between the storage material and the heat transfer fluid (HTF) and its
53 compatibility with the container material [22-25]. Finally, the choice of a storage material
54 strongly depends on the temperature level required for a kind of application [26].

55 Various systems related to sensible heat storage have been studied in the past. They may be
56 classified on the basis of the heat storage media as solid media storage and liquid media storage
57 [27]. Only some few studies have been conducted on combined solid/liquid media storage.

58 A variety of solid heat storage materials have been used as storage medium for high temperature
59 thermal energy storage, such as rocks, metals, concrete, sand, bricks etc. [27]. Among the
60 metals, aluminum, magnesium and zinc have been mentioned as suitable examples [27]. Metals
61 comprise high thermal conductivity and hence reduce the charging and discharging time. The
62 inconvenient of these materials is that they have low heat capacity, high density and high cost
63 that make these systems expensive to use. The use of metal media may be advantageous where
64 high thermal conductivity is required and where cost is of secondary importance [19]. Bricks,
65 concrete, graphite, etc. were studied as SHTS building materials and they are used to build
66 temperature controlled building [28-29]. For solar applications, most of the studies carried out
67 works with rocks and pebbles as packing materials [17]. This type of storage is very common
68 for high temperature applications (up to 1273 K) [30]. According to Laing et al. [31], castable
69 ceramic and high temperature concrete are also candidate storage materials and are suitable for
70 use in high temperature thermal storage in particular for solar applications. Some researchers
71 have carried out experimental works to compare the storage performances of solid materials.
72 For example, Rao et al. [5] have carried out experiments on lab-scale SHTS shell-and-tube heat
73 exchanger prototypes made up of cast steel and concrete at temperature range between 353 K
74 and 413 K. The thermal storage performances of such prototypes have been estimated at various
75 operating temperatures and HTF flow rates with respect to charging/discharging kinetics and
76 energy storage/discharge rates. This experimental study shows that, for the storage/discharge
77 phase, heat transfer rate is much better for cast steel prototype than for concrete prototypes due
78 to the higher thermal conductivity of cast steel. Some numerical works have also been done for
79 the purpose of comparing the storage performances of solid materials. For example, Prasad et
80 al. [32] have carried out a numerical investigation using COMSOL Multiphysics 4.2 to study
81 transient behavior and thermal storage capability of a cylindrical sensible heat storage unit at
82 temperature range between 523 K and 673 K. The cylindrical unit, which is embedded with
83 charging tubes, has been designed employing three different storage materials: concrete, cast
84 steel and cast iron. It was shown that the charging time for cast iron and cast steel are much less
85 than that of concrete. Charging time for concrete was reduced by 35.4% and 41.4% with
86 addition of 4 fins and 6 fins respectively.

87
88 Different kinds of liquids have also been used as sensible heat storage materials for low and
89 high temperature applications. Water, oil based fluids and molten salts are the most suitable
90 liquids [27]. Water is the most used for medium temperature applications (between 298 K and
91 363 K). In general, water exhibit a higher storing capacity than other materials, and it is cheap
92 and widely available [27], [33]. However, due to its high vapor pressure, water as heat storage
93 material requires insulation and pressure withstanding container for operation at high
94 temperature [19]. The most commonly proposed substitutes for water are molten salts. The heat
95 capacities are 25-40% of that of water on a weight basis. However, these substitutes have lower
96 vapor pressure than water and are able to operate at temperatures exceeding 573 K [27]. Molten
97 salts are the most widely studied and used in Concentrated Solar Plant (CSP) [34]. Some authors
98 choose to modify the properties of the liquid in order to improve its storage performance. El

99 Kaddadi et al. [35] carried out an experimental study of SHTS in a water/TiO₂ nanofluid
100 enclosed in an annular space in a vertical cylindrical system during a sensible heat storage cycle
101 (charging/discharging). From this study, it was found that the heat transfer was significantly
102 improved by using TiO₂-distilled water nanofluid. Furthermore, natural convection was
103 predominant in the vertical direction which would cause the thermal stratification. It was found
104 also that convective heat transfer coefficient has a strong influence on sensible heat storage
105 during a cycle (charging/discharging).
106

107 In the same spirit, the increase in performance can be obtained by combining solid/liquid heat
108 storage materials. Typical studies can be found in references [21] and [36] which rely on Harry
109 Thomason technique based on the use of both water and stone as storage media [21], [36]. The
110 high heat capacity of water, and the extensive area of the rock's container leads to efficient heat
111 transfer. Another study using combined thermal storage is presented by Moschatos [37]. In this
112 study, a type of TES that combines rock-bed and water storage is presented. Lugolole et al. [38]
113 have carried experimental tests to evaluate and compare three sensible heat thermal energy
114 storage systems during charging cycles. Two packed storage systems using Sunflower Oil as
115 the heat transfer fluid with two particle diameters (10.5 mm and 31.9 mm) are compared with
116 an oil only storage tank. The presence of pebbles of different sizes greatly modifies the
117 performance of the storage system by influencing the stored energy density and also the
118 charging and discharging dynamics.

119 The analysis of the above literature shows that very few studies have been focusing on the
120 development of combined solid/liquid media for sensible heat storage, especially for low
121 temperatures (273-300K). In addition, whatever the nature of the storage medium, the thermal
122 phenomena that drives the performance of the sensible storage systems during the dynamic
123 phases of charging and discharging are complex, dependent on the thermophysical properties
124 of the materials (storage material and heat transfer fluid) and also on the geometry of the various
125 components of the STHS system. Thus, the optimization of sensible storage systems that use
126 combination of solid and liquid materials is a difficult task that requires the analysis of complex
127 heat exchange during transient phases and parametric study of several geometries to propose
128 more efficient design. The use of CFD is required for this work due to the complexity of the
129 transient behaviour combining thermal storage in both solid (mainly conduction) and liquid
130 (natural convection) media, in order to analyse and optimise the performance of innovative
131 designs before manufacturing costly prototypes and performing validation tests. In agro-food
132 industry, the thermal conditioning of pressurized liquids, requires STHS system to overcome
133 load variability. A typical application is the distribution of draft beer that requires the use of an
134 efficient heat exchanger which also has a cold storage capacity to perfectly meet a large
135 variability of production. In this type of application, the heat exchanger that cools the food fluid
136 produced, should have an increased thermal inertia using a suitable thermal storage material.
137 The High Thermal Inertia Heat Exchanger (HTIHE) must therefore enable the thermal energy
138 to be transferred very quickly to the fluid that is cooled while allowing the cooling power
139 variations of the refrigerating system to be smoothed. This objective is usually reached by using
140 large metallic blocs to build the heat exchanger which increases its weight and cost. The aim of
141 this study is to numerically investigate the performances of an innovative SHTS system
142 combining a high thermal conductivity material (aluminium) and a high heat capacity material
143 (water) in order to enhance the storage performance and also decrease the weight and cost of
144 the system. Hence, a three-dimensional numerical comparison of the thermal behaviour of three
145 exchangers, is carried out under transient state conditions, for low temperature applications

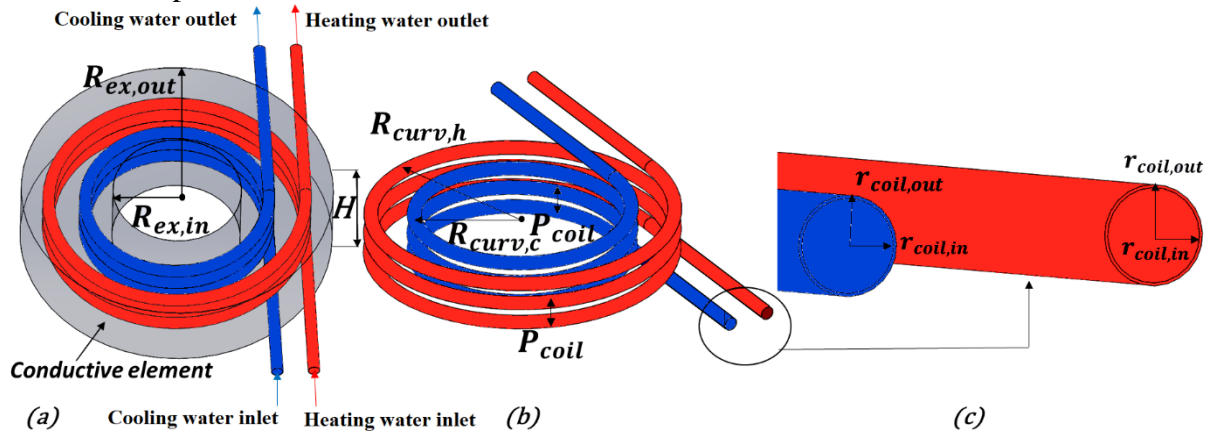
146 (273 K - 300 K). The developed model is used to identify and quantitatively evaluate the storage
 147 and the heat transfer performance of an innovative heat exchanger used in agro-food industry.

148 **2. Numerical analysis of the thermal energy storage**

149 In our study, in order to analyse the operation of this type of heat exchanger with high thermal
 150 inertia, a simplified geometry is used. This geometry is made of two coils inserted into a
 151 conductive solid element that will store some of the thermal energy (cold) in order to respond
 152 to variations in production. One of the two coils called “heating coil” conveys the fluid that
 153 must be cooled. Innovative designs of the High Thermal Inertia Heat Exchanger (HTIHE) using
 154 combination of solid and liquid storage material with natural convection are then studied in
 155 order to enhance its storage performance and decrease its weight and cost.

156 **2.1. Geometry description and boundary conditions**

157 The reference configuration (reference heat exchanger) is presented in Figure 1. It consists of
 158 two fluids (heating and cooling fluids) circulating in helical-shaped coils. Each coil consists of
 159 three turns. These coils are embedded in an aluminium cylindrical conductive element hollowed
 160 in its central part.



162 *Figure 1: (a) Illustration of the reference heat exchanger (b) Focus on the two coils (c) Details of the*
 163 *two fluid coils geometry*

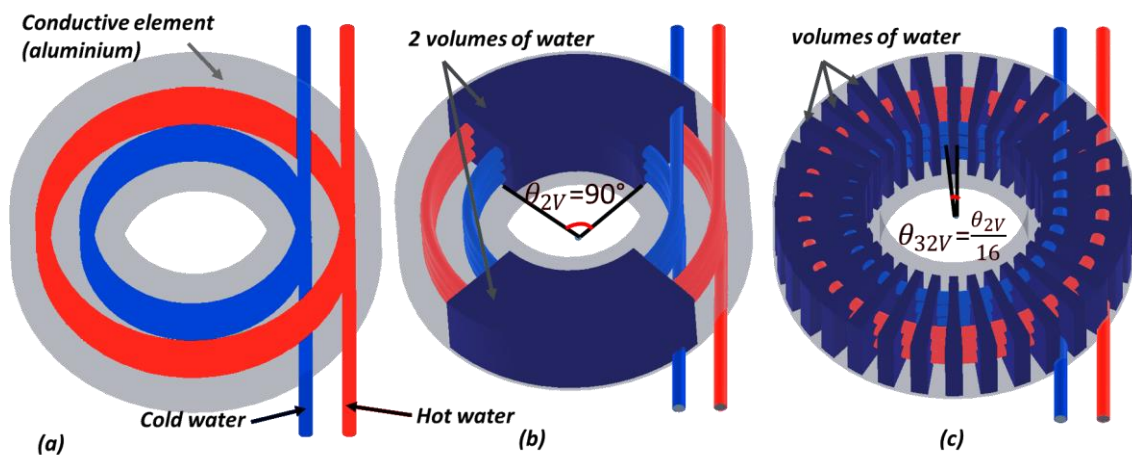
164 The aluminium cylindrical conductive element serves as a thermal storage medium during the
 165 transient operating phases. The coils are made of copper owing its high thermal diffusivity. The
 166 choice to use a helical geometry for the coils is related to a criterion of compactness.
 167 Furthermore, a helical configuration allows to intensify the heat transfer due to the development
 168 of the secondary flows of "Dean Cell" type within the fluid coils [39-40]. Table 1 summarizes
 169 the dimensionless parameters of the reference exchanger.

Conductive element			Helical coils			
$\frac{H}{r_{coil, in}}$	$\frac{R_{ex, in}}{r_{coil, in}}$	$\frac{R_{ex, out}}{r_{coil, in}}$	$\frac{r_{coil, out}}{r_{coil, in}}$	$\frac{P_{coil}}{r_{coil, in}}$	$\frac{R_{curv, c}}{r_{coil, in}}$	$\frac{R_{curv, h}}{r_{coil, in}}$
13.33	11.67	28.33	1.067	3.33	16.67	23.33

170
 171 *Table 1: Dimensionless parameters of the reference heat exchanger*

172 A second geometrical configuration of the heat exchanger is derived from the reference
 173 geometry by substituting a part of the conductive element with confined water volumes. This
 174 material substitution is operated while maintaining the same compactness compared to the
 175 reference configuration. The objective is to reduce the amount of conductive material

176 (Aluminium) with respect to the reference configuration while increasing the overall energy
 177 density of the heat exchanger that can be stored during transient operation phases.
 178 Figure 2b shows the second geometrical configuration for which a volume of the conductive
 179 material (Aluminium) has been replaced by an identical volume of water such as $V_w = V_{\text{alu, sub}} =$
 180 $V_{w1} + V_{w2}$. This second geometrical configuration will be called "configuration with two
 181 volumes of water" or C2V.
 182 A third geometrical configuration is derived from the above second configuration C2V by
 183 redistributing the two volumes of water into 32 elementary volumes in order to evaluate the
 184 influence of the spatial distribution of the confined water on the kinetics of thermal storage.
 185 Figure 2c shows the third geometrical configuration that will be called "configuration with 32
 186 volumes of water" or C32V. The geometrical configurations C2V and C32V have equal
 187 compactness, and equal overall sensible energy density during similar transient operation
 188 phases.
 189



190
 191 Figure 2: Illustration of the: (a) reference heat exchanger (b) heat exchanger C2V (c) heat exchanger
 192 C32V

193 Numerical simulations were carried out for the three heat exchangers in steady state, and in
 194 transient regime. A phase of charge as well as a phase of discharge of cold were thus tested in
 195 order to characterize the kinetics of heat transfer for the different configurations.
 196

197 2.2. Initial and boundary conditions

198
 199 In order to analyse the heat transfer and the kinetics of thermal energy storage, real operating
 200 conditions of such exchangers have been chosen by considering classically application
 201 encountered in agro-food industry such as the thermal conditioning of beverage. In such
 202 application, it is important to study both the charging and discharging phases since the
 203 efficiency of a heat exchanger in such applications depends on the charge/discharge kinetics.
 204 Different scenarios have then been studied.

205 2.2.1. Steady state operation

206 At the inlets of the heating and the cooling heat transfer fluids circulating in the coils, Poiseuille
 207 velocity profiles corresponding to mean inlet velocities of about $U_{w,in} = 0.21; 0.31$ and 0.41 m.s^{-1}
 208 are imposed. These mean velocities correspond respectively to Reynolds numbers of about
 209 $Re_{\text{dcoil,in}} = 1000; 1500$ and 2000 based on the inner diameter of the coils are imposed. It has to
 210 be noted that Reynolds numbers are not exactly the same for the same velocity of the cooling
 211 and the heating fluids due to difference in viscosity for the two heat transfer fluids. It has been
 212 chosen to carry out the study at constant velocities of the heating and the cooling fluids to

213 comply with real operating conditions of an exchanger in agro-food industry where the flowrate
214 is of great importance. Constant inlet temperatures $T_{in,h} = 295$ K and $T_{in,c} = 275$ K are
215 respectively imposed at the inlet of the heating and the cooling fluids. At the outlets of the
216 heating transfer fluids, pressure outlet boundary condition is considered. At all fluid-solid and
217 solid-solid interfaces, conjugate heat transfer is considered. All the external boundaries of the
218 conductive element are adiabatic.

219 **2.2.2. Transient state operation**

220 In transient state operation, two operating phases were considered namely:

- 221 • A charging phase
- 222 • A discharging phase

223 During the charging phase, it is considered that the heat exchanger is subjected only to the
224 thermal influence of the cooling heat transfer fluid. The heating heat transfer fluid is therefore
225 stagnant in the coil. The single circulation of the cooling heat transfer fluid corresponds to the
226 charge of cold energy inside the heat exchanger. The following initial and boundary conditions
227 are considered during this phase.

228 ○ Initial conditions

229 At the initial time, all the heat exchanger volume (conductive element, volumes of confined
230 heat transfer fluid, heating and cooling heat transfer fluids in the coils) is supposed to be at an
231 initial uniform temperature $T_i(x, y, z, 0) = 295$ K.

232 ○ Boundary conditions

233 As the heating heat transfer fluid is stagnant, a velocity inlet $U_{w,in} = 0$ m.s⁻¹ and a pressure outlet
234 boundary conditions are respectively imposed at the inlet and at the outlet of the heating heat
235 transfer fluid.

236 At the inlet of the cooling heat transfer fluid, Poiseuille velocity profiles corresponding to mean
237 inlet velocities $U_{w,in} = 0.21$ m.s⁻¹ and 0.41 m.s⁻¹ are imposed. A constant inlet temperature $T_{in,c}$
238 = 275 K is imposed at the inlet of the cooling heat transfer fluid while a pressure outlet boundary
239 condition at the outlet is considered. At all fluid-solid and solid-solid interfaces, conjugate heat
240 transfer is considered. All the external boundaries of the conductive element are adiabatic.

241 During the discharging phase, it is considered that the heat exchanger is subjected only to the
242 thermal influence of the heating heat transfer fluid. The cooling heat transfer fluid is therefore
243 stagnant in the coil.

244 ○ Initial conditions

245 At the initial time, all the heat exchanger volume (conductive element, volumes of confined
246 heat transfer fluid, heating and cooling heat transfer fluids in the coil) is supposed to be at an
247 initial uniform temperature $T_i(x, y, z, 0) = 275$ K.

248 ○ Boundary conditions

249 As the cooling heat transfer fluid is stagnant, a velocity inlet $U_{w,in} = 0$ m.s⁻¹ and a pressure outlet
250 boundary conditions are respectively imposed at the inlet and at the outlet of the cooling heat
251 transfer fluid.

252 At the inlet of the heating heat transfer fluid, Poiseuille velocity profiles corresponding to mean
253 inlet velocities $U_{w,in} = 0.21$ m.s⁻¹ and 0.41 m.s⁻¹ are imposed. A constant inlet temperature $T_{in,h}$
254 = 295 K is imposed at the inlet of the heating heat transfer while at the outlet, a pressure outlet
255 boundary condition is considered. At all fluid-solid and solid-solid interfaces, conjugate heat
256 transfer is considered. All the external boundaries of the conductive element are adiabatic.

257 For all simulations performed in this study, the thermo-physical properties of water, copper and
258 aluminium are evaluated at an average temperature of 285 K.

259
260

261 **2.3. Physical formulation**

262

263 The flow in the different heat exchanger configurations is modelled through the conservation
 264 equations (mass, momentum) in a laminar regime using water as working fluid which is
 265 considered incompressible and viscous. The heat transfer is modelled through the energy
 266 equation for the heat transfer fluids circulating in the coils, coupled with the thermal diffusion
 267 equation in the coils tube made of copper and in the conductive element made of aluminium.
 268 In addition, natural convection phenomena are taken into account in the confined heat transfer
 269 fluid (in C2V and C32V) through the Boussinesq approximation and neglected in the circulating
 270 heat transfer fluids. The viscous heating in the fluids is neglected. By considering the above
 271 assumption, the conservation equations modelling the flow and heat transfer in the exchanger
 272 can be written as follow:

273

- 274 • Circulating heat transfer fluids (Water)

$$275 \quad \frac{\partial \rho_w}{\partial t} + \nabla \rho_w \cdot \vec{V} = 0 \quad (1)$$

$$276 \quad \rho_w \frac{\partial \vec{V}}{\partial t} + \rho_w (\vec{V} \cdot \nabla) \vec{V} = -\nabla P + \mu_w \nabla^2 \vec{V} \quad (2)$$

$$277 \quad \rho_w C_{p,w} \frac{\partial T}{\partial t} + \rho_w C_{p,w} \vec{V} \cdot \nabla T = \lambda_w \nabla^2 T \quad (3)$$

- 278 • Coils tube (Copper)

$$279 \quad \rho_{cop} C_{p,cop} \frac{\partial T}{\partial t} = \lambda_{cop} \nabla^2 T \quad (4)$$

280

- 281 • Conductive element (Aluminium)

$$282 \quad \rho_{Al} C_{p,Al} \frac{\partial T}{\partial t} = \lambda_{Al} \nabla^2 T \quad (5)$$

- 283 • Confined heat transfer fluid (Water)

$$284 \quad \frac{\partial \rho_w}{\partial t} + \nabla \rho_w \cdot \vec{V} = 0 \quad (6)$$

$$285 \quad \rho_w \frac{\partial \vec{V}}{\partial t} + \rho_w (\vec{V} \cdot \nabla) \vec{V} = -\nabla P + \mu_w \nabla^2 \vec{V} + \rho_w \vec{g} \beta (T_{ref} - T) \quad (7)$$

$$286 \quad \rho_w C_{p,w} \frac{\partial T}{\partial t} + \rho_w C_{p,w} \vec{V} \cdot \nabla T = \lambda_w \nabla^2 T \quad (8)$$

287 **3. Numerical procedure**

288

289 **3.1. Numerical scheme and solvers**

290

291 The commercial code STAR-CCM + V12.02 [41] was used to solve the conservation equations
 292 based on a finite volume discretization method. The conservation equations were solved
 293 sequentially using the AMG algebraic solver and the SIMPLE algorithm for pressure-velocity
 294 coupling. A second-order discretization was chosen for the convective terms of the momentum
 295 and energy equations. A temporal discretization of second order was chosen.

296

297 **3.2. Grid and time step sensitivity study**

298

299 A grid sensitivity study was carried out in steady state for the reference heat exchanger
 300 configuration for a mean inlet velocity $U_{w,in} = 0.21 \text{ m.s}^{-1}$ corresponding to Reynolds number
 301 $Re_{coil,in}$ of about 1000 imposed in the inlet of the heating and the cooling heat transfer fluids.

302 The appropriate grid was chosen based on two global indicators namely the heat duty of the
303 heat exchanger and the pressure drop in the heating coil.

304 By performing a gradual refinement of the mesh, a set of four grid systems having respectively
305 2.5; 3.5; 4.9 and 6.6 Million of cells were generated in the computational domain. The
306 difference in the heat duty and the pressure drop between the grid system with 4.9 Million and
307 the one with 6.6 Million of cells did not exceed respectively 1.5 % and 1 %. Taking into account
308 the available computing resources, it was decided to use the configuration having 4.9 Million
309 cells throughout the study.

310 Figure 3 illustrates the retained grid distribution in the vertical median plane for the reference
311 geometry presented only on the right side of the plane. Polyhedral meshes were used for the
312 aluminium region. For copper region, the “thin layer mesher” [41] was used. This type of mesh
313 is typically used in order to generate a prismatic type volume mesh for thin volumes within
314 parts or regions [41] of the computational domain. For the heating and the cooling heat transfer
315 fluids circulating in the coils, advancing layer mesher [41] was used. This type of mesh
316 generates layers of prismatic cells around the surfaces of regions or parts and fills the remaining
317 void with polyhedral cells [41]. Some advantages of this approach are a conformal match on
318 either side of an interface [41] which is crucial for conjugate heat transfer.

319 It is important to note that the grid distribution for the C2V and C32V configurations are not
320 presented in order to save space. However, the same types of meshes were used for aluminium,
321 copper and circulating fluids as for the reference. These two configurations, are derived from
322 the reference geometry by substituting a part of the conductive element (aluminium) with
323 confined water volumes as mentioned in section 2.1. For these confined water volumes, the
324 trimmed cell mesher which generates hexahedral cells was used. Attention was paid to near
325 wall grid structure using a progressive refinement in the vicinity of walls in order to correctly
326 capture near wall high velocity and temperature gradients.

327

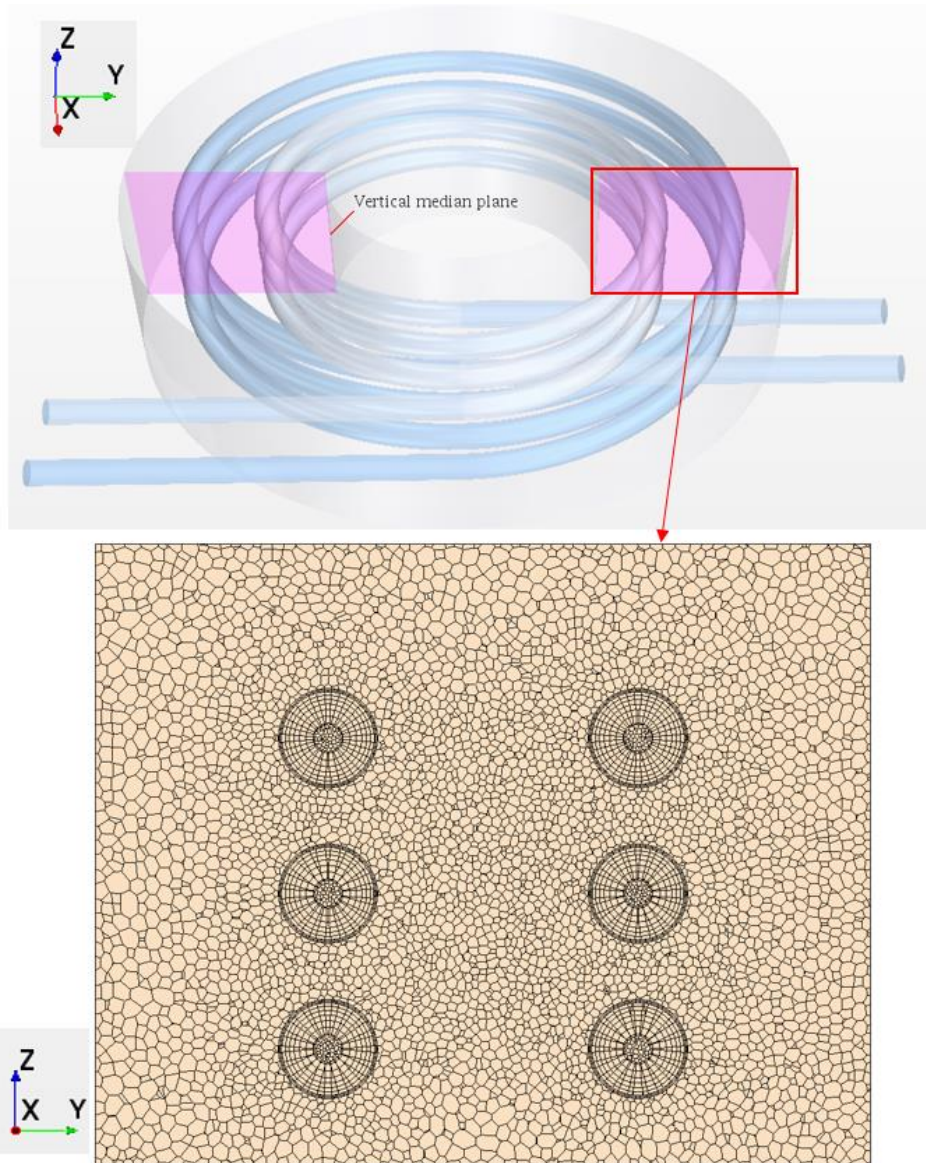


Figure 3: Grid distribution in the vertical median plane for the reference geometry

328
329

330 Moreover, since the precision of the results is intimately related to the time step chosen for
 331 unsteady calculations, a time step sensitivity study was carried out using the optimal above grid
 332 and a succession of three time steps of 0.5 s; 0.1 s and 0.05 s. This study led to the use of an
 333 adaptive time step of 0.05 s during the flow development time in the coils followed by a time
 334 step of 0.1 s for the rest of the charging (or discharging) phase for the lowest Reynolds number
 335 $Re_{dcoil,in}$ of about 1000. For the highest Reynolds number $Re_{dcoil,in}$ of about 2000, an adaptive
 336 time step of 0.025 s during the flow development time and then a time step of 0.05 s for the rest
 337 of the charging (or discharging) phase have been chosen. For this highest Reynolds number,
 338 the time steps were divided by 2 compared to the lowest Reynolds number in order to maintain
 339 an equal courant number (CFL) for the both cases.

340

341 3.3. Numerical validation

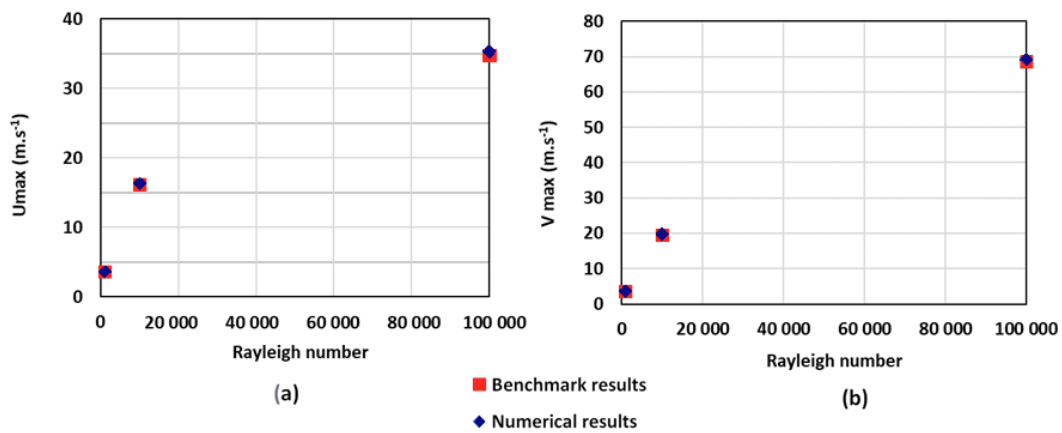
342

343 In order to validate the physical models and the ability of the CFD code to correctly predict the
 344 major physical phenomena involved in the system, a numerical simulation of the natural
 345 convection in a square cavity was carried out, in steady state, in the same geometrical
 346 configuration as that studied by De Vahl Davis [42] and for fixed temperatures equal to 275 K

347 for the cold vertical wall and 295 K for the hot vertical wall, the horizontal walls being adiabatic
 348 and having variable cavity size.

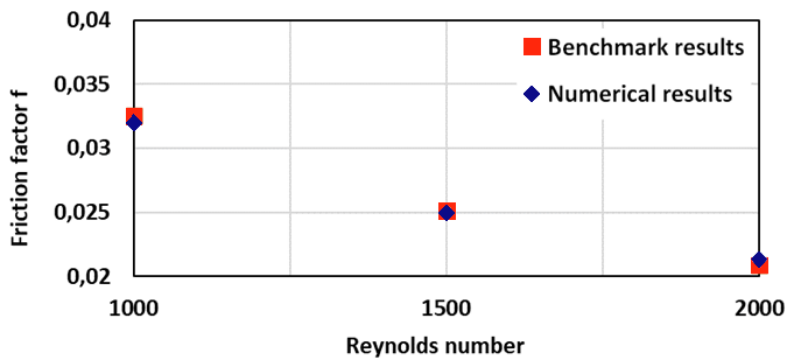
349 Figures 4a and 4b compare respectively the evolution of the maximum x-velocity and the
 350 maximum y-velocity on a centre vertical line in the cavity between the present study and the
 351 one of Davis [42]. These figures clearly show a good match between both studies with a
 352 maximum discrepancy of 1.7% for the maximum x-velocity and a maximum discrepancy of
 353 1.8% for the maximum y-velocity thus validating the numerical procedure for natural
 354 convection. Similarly, a numerical simulation of flow characteristics in the coils was also
 355 performed by considering a water flow in a helical coil, and compared to Prandtl correlation
 356 [43] evaluating the friction factor in a helical coil.

357 As in presented in figure 5, the results showed a difference in the prediction of friction between
 358 the present study and the Prandtl correlation [43] that did not exceed 2.5 % for Reynolds
 359 numbers varying from 1000 to 2000 thus validating the numerical procedure for the flow
 360 characteristics in the coils.



361
 362 *Figure 4: Validation of the natural convection based on de Vahl Davis study [42]*

363



364
 365 *Figure 5: Validation of the flow characteristics in the coils with the Prandtl correlation [43]*
 366

367 **4. Results**

368 In this section, firstly, results obtained in steady state operation for the three exchangers are
 369 presented. Then, the detailed results in transient state operation are presented and discussed
 370 from qualitative and quantitative, local and global points of views. An analysis of the local
 371 mechanisms of conducto-convective heat transfer is performed followed by an analysis of
 372 global heat transfer performance with a focus on the heat transfer kinetics for transient studies.
 373

374 **4.1. Steady state operation of the heat exchangers**

375 In steady state, a comparison of the heat duty exchanged between the two coils for the three
376 exchangers (reference, C2V and C32V) was performed for a laminar flow regime. Three mean
377 inlet velocities were investigated: $U_{w,in} = 0.21; 0.31$ and 0.41 m.s^{-1} . Table 2 summarizes steady-
378 state results.

Mean inlet velocity(m.s^{-1})	Reference config.	Config. C2V	Config. C32V
0.21	207.01	164.63	194.67
0.31	283.99	214.49	260.61
0.41	347.66	260.61	312.71

379 *Table 2 : Heat duty (W) exchanged in the three heat exchanger configurations for different mean inlet*
380 *velocities*

381 For the three configurations tested, the heat duty exchanged between the coils increases with
382 increasing the mean inlet velocity and therefore the Reynolds number. The heat duty exchanged
383 is more important for the reference configuration followed by the C32V configuration and the
384 C2V configuration. Consequently, the spatial redistribution of the two water volumes of the
385 C2V configuration into 32 volumes leads to achieve better performances where values of heat
386 transfer are close to the reference configuration despite the substitution of 41.3% of conductive
387 material by a less conductive material (water). This substitution leads also to a significant
388 material saving.

389 Since this study is intended to study the thermal storage, we will focus, in the following, on the
390 transient operation of the heat exchangers due to the fact that the unsteady state operation is of
391 capital importance for sensible heat storage.

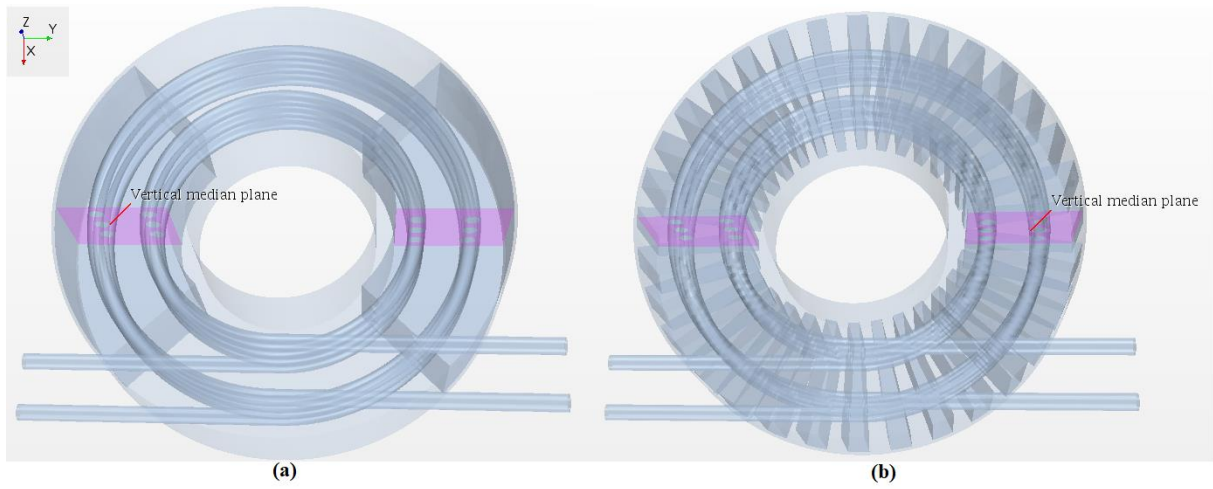
392 **4.2. Local mechanisms of conducto-convective heat exchanges in transient operation**

393 The transient behaviour of the heat exchanger is of primer importance. The aim is to design an
394 innovative High Thermal Inertia Heat Exchanger (HTIHE) with a lower mass of the conductive
395 material compared to the reference while keeping quasi-equivalent transient behaviour and
396 higher thermal storage performance. This part of the analysis will focus on the presentation of
397 the local heat transfer mechanism that occurs in the two innovative designs. Contours of
398 temperature and velocity at three different times during the charging phase as well as the
399 discharging phase for different Reynolds numbers will be presented. The velocity contours are
400 presented since they provide information on the intensity of natural convection in confined heat
401 transfer fluid (water) for the C2V and C32V configurations and thus information on the charge
402 / discharge kinetics.

403 **4.2.1. Charging phase of the cold**

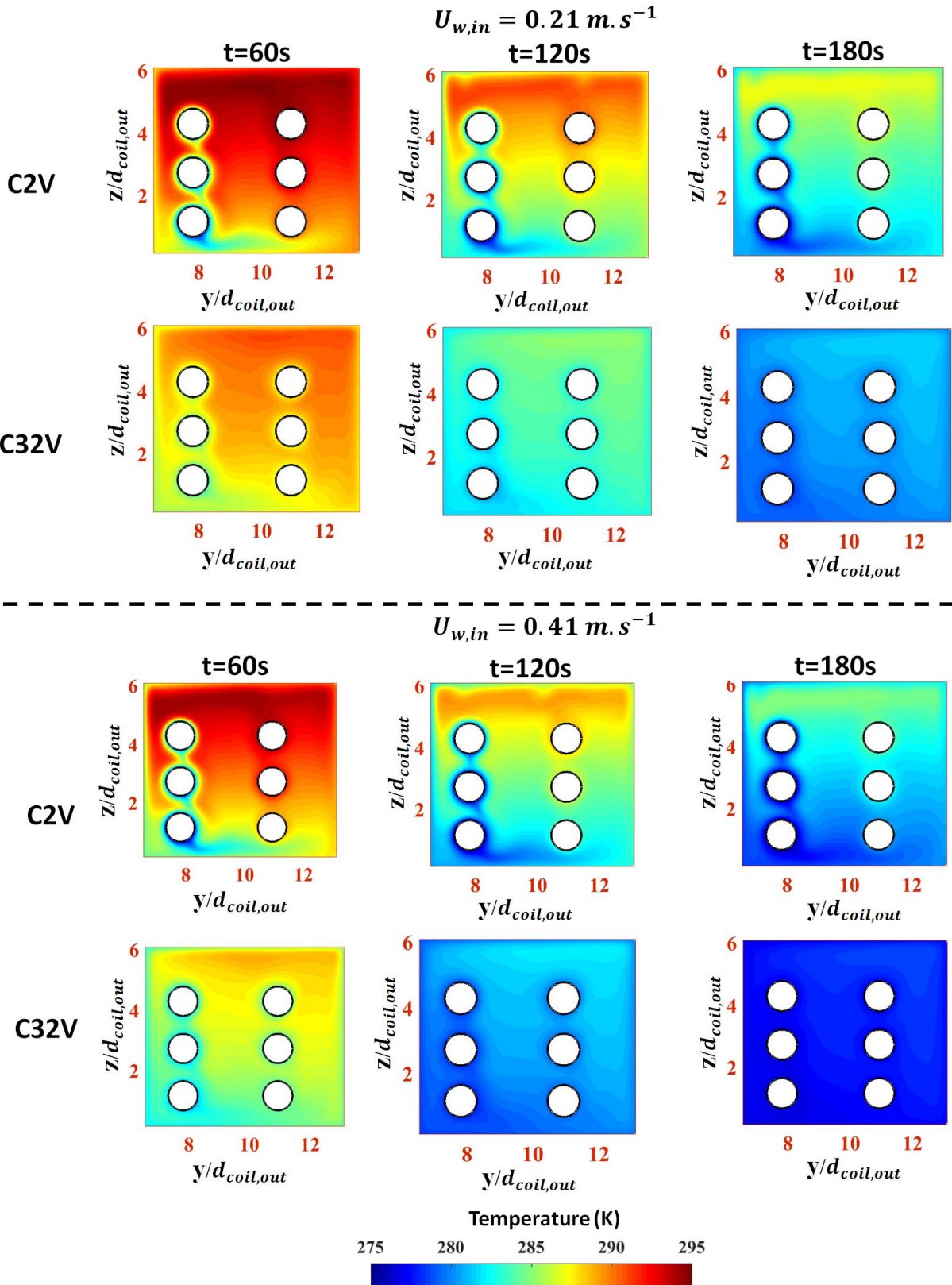
404 In order to analyse the local mechanism of heat transfer in the HTIHE, temperature and velocity
405 maps are presented in a vertical median plane passing through the center of a volume of
406 confined water heat transfer fluid for C2V and C32V configurations at three different times
407 during the charging phase respectively for two mean inlet velocities: $U_{w,in} = 0.21$ and 0.41 m.s^{-1}
408 ¹ in the cooling coil. Figure 6 illustrates the vertical median plane and results are presented only
409 on the right side of the plane. The heat transfer fluid is at rest in the heating coil.

410



411
412
413
414

Figure 6 : Illustration of the vertical median plane for C2V configuration (a) and C32V configuration (b)

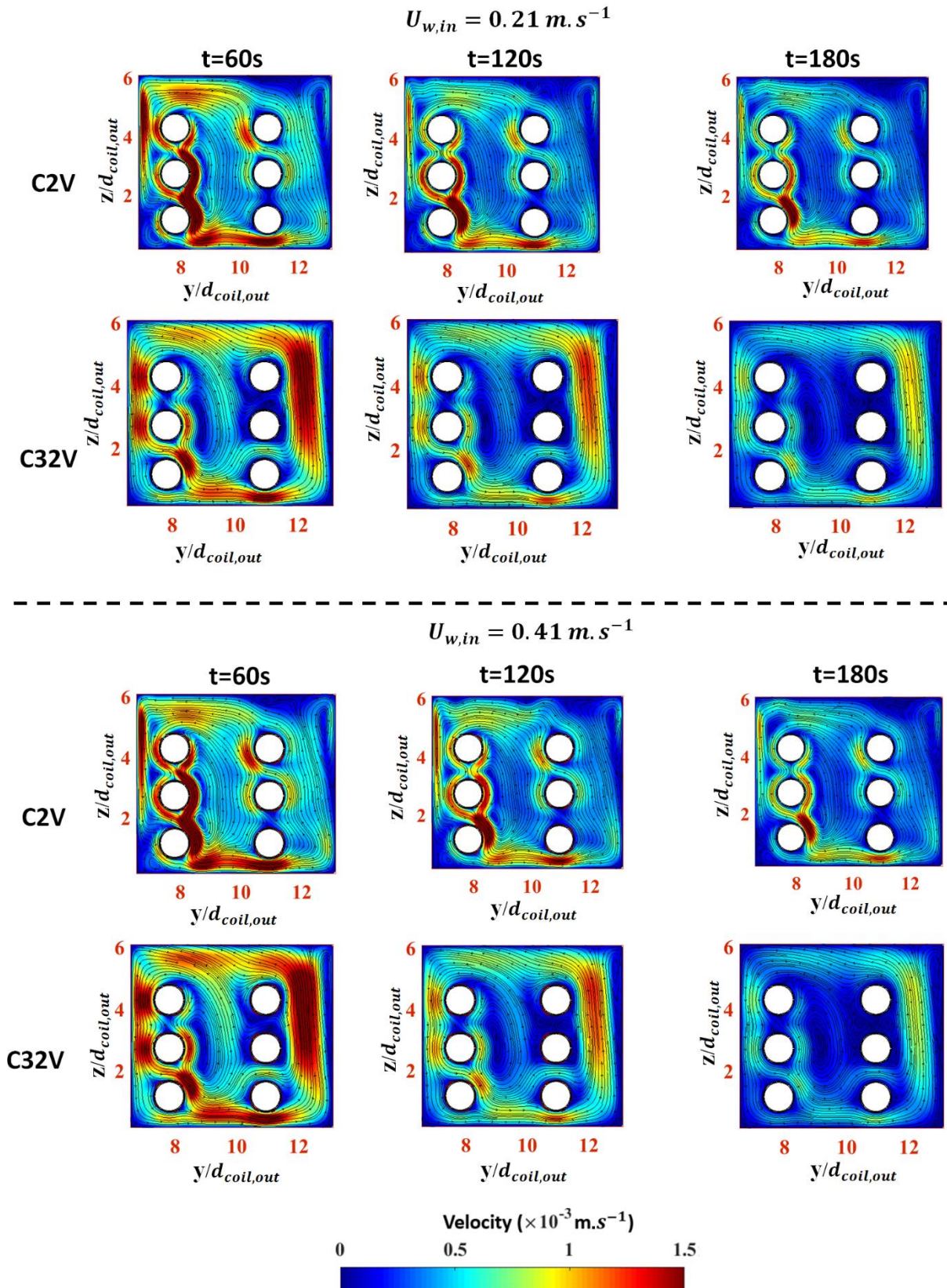


415

416 *Figure 7 : Temperature (colour level) contours for two mean inlet velocities of $U_{w,in} = 0.21$ and*
 417 *0.41 m.s^{-1} in the cooling coil during the charging phase*

418

419



420
421
422
423
424
425
426

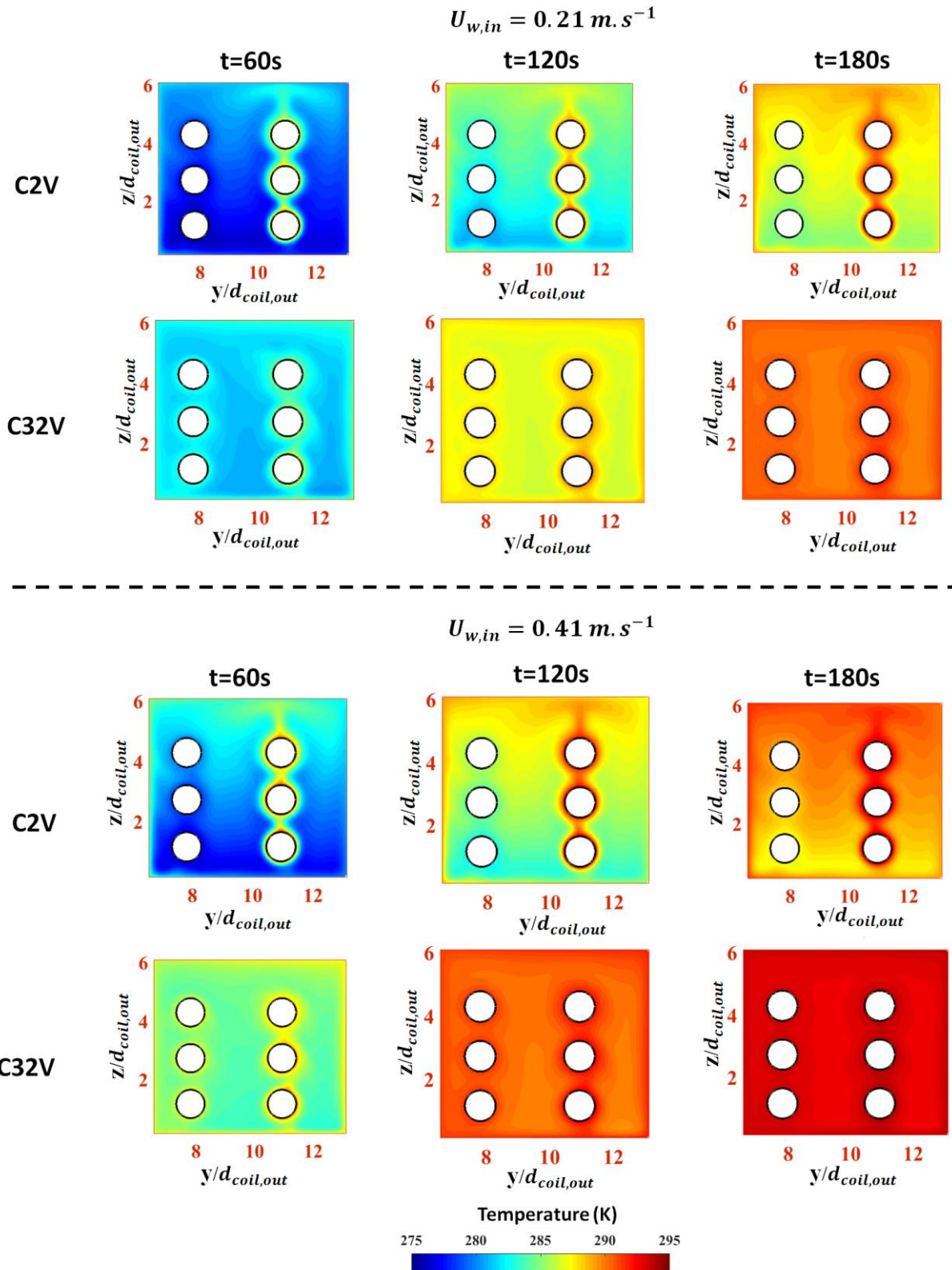
Figure 8 : Velocity (colour level and vector field) contours for two mean inlet velocities of $U_{w,in} = 0.21$ and 0.41 m.s^{-1} in the cooling coil during the charging phase

Figure 7 and 8 show respectively the contours of temperature and velocity at $t=60 \text{ s}$, 120 s and 180 s during the charging phase for two mean inlet velocities of $U_{w,in} = 0.21$ and 0.41 m.s^{-1} in the cooling coil. Both C2V and C32V HTIHE configurations have initially a uniform

427 temperature $T_i(x, y, z, 0) = 295$ K. Imposing a constant temperature condition $T_{in,c}(x, y, z, t)$
428 $= 275$ K at the inlet of the cooling coil induces the appearance of local temperature (and
429 correspondingly velocity) gradients in the confined water HTF that put the fluid into motion.
430 The local temperature maxima are higher at each time for C2V configuration compared to the
431 C32V configuration indicating a faster cold charging kinetics for C32V configuration compared
432 to C2V. The temperature gradients observed in the confined water heat transfer fluid induce a
433 thermal storage because of the fluid motion generated by buoyancy forces.
434 It is noted that increasing the mean inlet velocity and therefore the Reynolds number is followed
435 by a faster cold charging kinetics. Indeed, the temperature field is quite uniform after 120
436 seconds in C32V configuration for a mean inlet velocity of $U_{w,in} = 0.41$ m.s⁻¹ in the cooling coil
437 while this quasi-uniformity is not yet reached at 180s for the same configuration for a mean
438 inlet velocity of $U_{w,in} = 0.21$ m.s⁻¹ in the cooling coil. The same qualitative conclusion is
439 observed for C2V however with higher temperature gradients compared to C32V. For both
440 configurations, as the storage of cold proceeds, temperature gradients decrease leading to
441 velocity gradients decrease because of the diminution of the buoyancy forces in the course of
442 time. This decrease is higher in C32V configuration compared to C2V configuration supporting
443 once more the faster charging kinetics in C32V configuration.
444

445 ***4.2.2. Discharging phase of the cold***

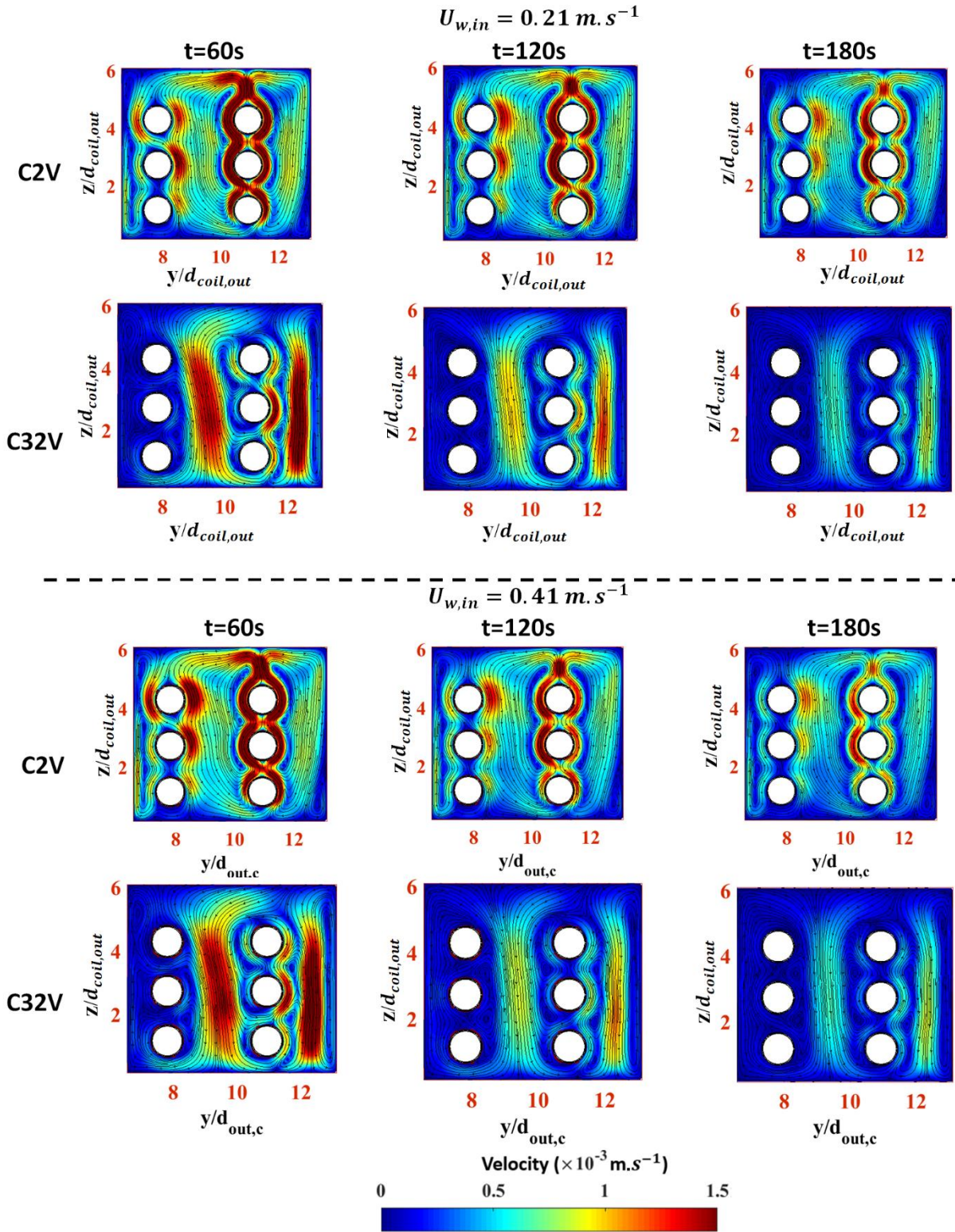
446 In order to analyse the local mechanism of heat transfer in the HTIHE, temperature and velocity
447 maps are presented in a vertical median plane passing through the center of a volume of water
448 (see figure 6) for C2V and C32V configurations at three different times during the discharging
449 phase respectively for two mean inlet velocities: $U_{w,in} = 0.21$ and 0.41 m.s⁻¹ in the heating coil.
450 The heat transfer fluid (HTF) is at rest in the cooling coil.
451
452



453
454
455

Figure 9: Temperature (colour level) contours for two mean inlet velocities: $U_{w,in} = 0.21$ and $0.41 \text{ m} \cdot \text{s}^{-1}$ in the heating coil during discharging phase

456
457
458
459



460

461 *Figure 10: Velocity (colour level and vector field) contours for two mean inlet velocities: $U_{w,in} = 0.21$*
 462 *and 0.41 m.s^{-1} in the heating coil during the discharging phase*

463 Figure 9 and 10 show respectively the contours of temperature and velocity at $t=60 \text{ s}$, 120 s and
 464 180 s during the discharging phase. Both heat exchangers have initially a uniform temperature
 465 $T_i(x, y, z, 0) = 275 \text{ K}$. Imposing a constant temperature condition $T_{in,h}(x, y, z, t) = 295 \text{ K}$ at the
 466 inlet of the heating coil induces the appearance of local temperature gradients (and
 467 correspondingly velocity gradients) in the confined water HTF that put the fluid into motion.

468 The local temperature maxima are higher at each instant for C32V configuration compared to
 469 C2V configuration indicating a faster cold discharging kinetics for C32V configuration
 470 compared to C2V configuration.

471 It is noted that increasing the mean inlet velocity and therefore the Reynolds number in the
 472 heating coil is followed by a faster discharging kinetics. Indeed, the temperature field is quite
 473 uniform after 120 seconds in C32V configuration for a mean inlet velocity of $U_{w,in} = 0.41 \text{ m.s}^{-1}$
 474 ¹ in the heating coil while this quasi-uniformity is not yet reached at 180s for the same
 475 configuration for a mean inlet velocity of $U_{w,in} = 0.21 \text{ m.s}^{-1}$ in the heating coil. The same
 476 qualitative conclusion is observed for C2V however with higher temperature gradients
 477 compared to C32V. Velocity gradients remain low despite doubling the velocity of the heating
 478 heat transfer fluid.

479 For both configurations, as the release of cold proceeds, temperature gradients decrease leading
 480 to velocity gradients decrease because of the diminution of the buoyancy forces in the course
 481 of time. This decrease is higher in C32V configuration compared to C2V configuration
 482 supporting once more the faster discharging kinetics in C32V configuration.

483

484 **4.3. Global analysis of conducto-convective heat exchanges and storage performances in**
 485 **transient operation**

486 This part of the analysis will focus on the presentation of the global results and performances
 487 in the Reynolds numbers range studied for the charging and discharging phases. As one of the
 488 aim of the study is to save the conductive material in modified HTIHE configurations (C2V
 489 and C32V) with respect to the reference geometry while increasing their potential of thermal
 490 energy storage, table 3 compares the three configurations in terms of mass and overall energy
 491 density. The material saving and the energy density increase are computed with respect to the
 492 reference configuration.

Configuration	Mass (kg)	Mass reduction (%)	Material saving (%)	Energy density (J. K^{-1})	Energy density increase (%)
Reference	1.91	-	-	1680	-
C2V	1.44	24.6%	41.3%	2160	28.57%
C32V	1.44	24.6%	41.3%	2160	28.57%

493 *Table 3: Comparison of the three configurations*

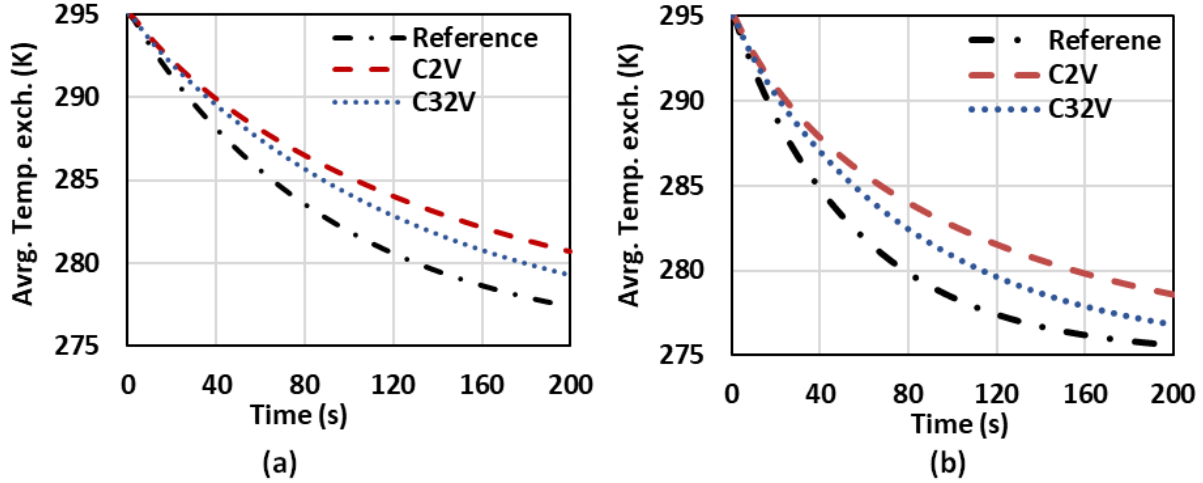
494 As it can be noted, the two HTIHE configurations C2V and C32V are better than the reference
 495 case not only in terms of overall energy density, but also in terms of material saving. In order
 496 to compare the storage performance of the two innovative configurations with the reference
 497 case, the following results focus on the analysis of their thermal response during the charging
 498 and discharging periods.

499

500 **4.3.1. Charging phase of cold**

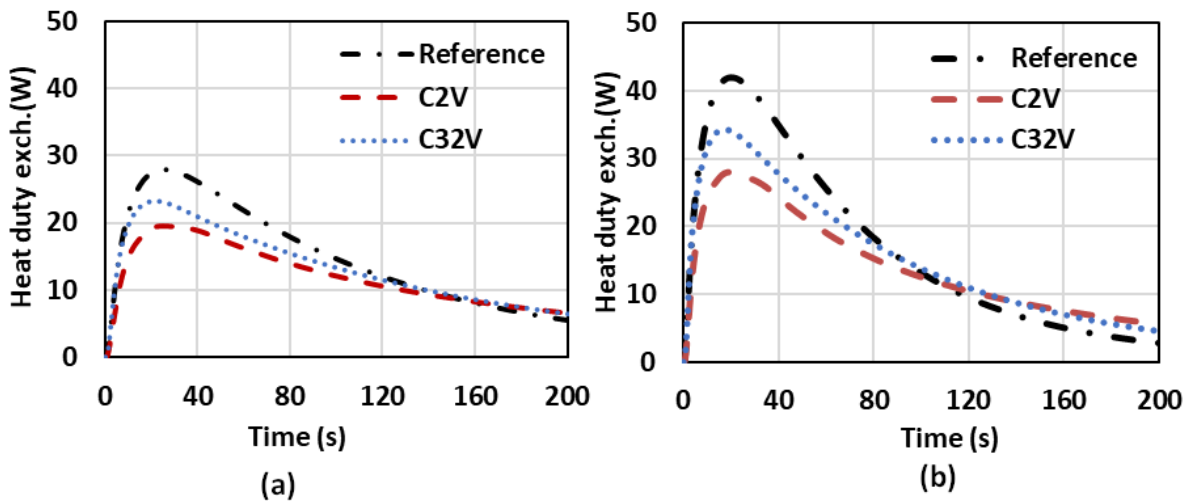
501 The charging time, overall weight and energy density are important parameters to be taken into
 502 consideration in classical use of the HITHE in agro-food applications such as beverage cooling
 503 with easy handling cooling units. Figure 11 shows the temporal evolution of the average heat
 504 exchangers temperature for the three configurations during the first 200 seconds of charge
 505 respectively for mean inlet velocities values of $U_{w,in} = 0.21$ and 0.41 m.s^{-1} in the cooling coil.
 506 These mean velocities correspond respectively to Reynolds numbers of about $Re_{dcoil,in} = 1000$
 507 and 2000. The heating heat transfer fluid is therefore stagnant in the heating coil. The average
 508 heat exchanger temperature is calculated as the average volumetric temperature of the storage
 509 medium (i.e. the aluminium for the reference configuration and the aluminium with the

510 confined water HTF for C2V and C32V configurations). In the above intended application, the
 511 HTIHE must reach the lowest temperature level in minimum time. Figure 11b shows that for
 512 the highest value of mean inlet velocity $U_{w,in} = 0.41 \text{ m.s}^{-1}$, the time needed to reach a
 513 temperature level of 280 K is 80s, 115s and 160s respectively for the reference, C32V and C2V
 514 HTIHE geometries indicating charging kinetics slightly lower for C2V and C32V
 515 configurations than the reference case. The same conclusion is made for the lowest value of
 516 mean inlet velocity $U_{w,in} = 0.21 \text{ m.s}^{-1}$ (see figure 11a). This trend is clearly due to the high
 517 overall diffusivity of the reference geometry compared to the innovative ones.



518
 519 *Figure 11: Temporal evolution of the average temperature of the exchangers for $U_{w,in} = 0.21 \text{ m.s}^{-1}$*
 520 *(a) and $U_{w,in} = 0.41 \text{ m.s}^{-1}$ (b) in the cooling coil*

521 Nevertheless, it is worth to mention that, despite 41.3% aluminium substitution with stagnant
 522 low conductivity water HTF corresponding to 28.57% increase of the energy density in C2V
 523 and C32V configurations, the redistribution of the confined water HTF into small volumes
 524 embedded in the aluminium bloc leads to a significant increase of the cooling kinetics in the
 525 C32V configuration compared to the C2V configuration.



526
 527 *Figure 12 : Temporal evolution of the heat duty exchanged with the stagnant heating fluid in the coil*
 528 *for $U_{w,in} = 0.21 \text{ m.s}^{-1}$ (a) and $U_{w,in} = 0.41 \text{ m.s}^{-1}$ (b) in the cooling coil*

529 Figure 12 shows the temporal evolution of heat duty exchanged with the stagnant heating fluid
 530 in the coil for mean inlet velocities values of $U_{w,in} = 0.21$ and 0.41 m.s^{-1} in the cooling coil (the
 531 heating fluid does not flow during the charging phase of cold). The results are in agreement

532 with the above discussion from figure 11 showing the temporal evolution of the average heat
 533 exchangers temperature. Indeed, the heat duty exchanged with the stagnant heating fluid
 534 exhibits during the first instants of time a peak value, higher for the reference heat exchanger
 535 followed by C32V and then C2V. The trend is reversed from $t=160$ s for $U_{w,in} = 0.21$ m.s⁻¹
 536 (figure 12a) and from $t=100$ s for $U_{w,in} = 0.41$ m.s⁻¹ (figure 12b) and the heat duty exchanged
 537 with the stagnant heating fluid is higher for configurations C32V and C2V compared to the
 538 reference. This is mainly due to the fact that configurations C2V and C32V have an overall
 539 higher energy density than the reference. Furthermore, more homogeneous spatial distribution
 540 of the confined water volumes makes heat transfer faster in the C32V configuration than in the
 541 C2V configuration.

542 In order to better study the advantages obtained by the geometrical configuration C32V
 543 compared to C2V configuration, a fine analysis of heat transfer is carried out in the confined
 544 water HTF volumes.

545 The maximum energy that can be stored in confined water volumes can be calculated from the
 546 change in enthalpy when cooling the confined water HTF from the initial temperature $T_w(t_0)$
 547 (295 K at initial time $t_0=0$ s) to the final temperature $T_w(t_f)$ (275 K at final time $t_f = \infty$) from the
 548 following equation:

$$549 \quad E_{tot,w} = \rho_w C_{p,w} V_w [T_w(t_0) - T_w(t_f)] \quad (9)$$

550 In this equation, ρ_w , $C_{p,w}$ and V_w represent respectively the density, the specific heat and the
 551 total volume of water confined in the conductive element.

552 Similarly, the volumetric power locally stored in each cell of confined water HTF volumes can
 553 be deduced from the energy equation as follows:

$$554 \quad \underbrace{\rho_w C_{p,w} \frac{\partial T}{\partial t}}_{\text{Storage-term}} = \underbrace{\lambda_w \nabla^2 T}_{\text{Conduction-term}} - \underbrace{\rho_w C_{p,w} \vec{V} \cdot \nabla T}_{\text{Convection-term}} \quad (10)$$

555 The thermal power stored at each time in the confined water HTF total volume can be evaluated
 556 by integrating the storage term of the above equation into the total volume of water as follows:

$$557 \quad P_{vol,w} = \int \rho_w C_{p,w} \frac{\partial T}{\partial t} dV \quad (11)$$

558 The cooling energy stored by confined water volumes can therefore be deduced from the power
 559 exchanged by simple temporal integration between the initial charging time $t_0=0$ s and any time
 560 t as follows:

$$561 \quad E_{csw} = \int_{t_0}^t P_{vol,w} dt \quad (12)$$

562 A cooling charge ratio in the confined water HTF volumes can be defined as follows:

$$563 \quad R_{cc} = \frac{E_{csw}}{E_{tot,w}} \cdot 100 \quad (13)$$

564 Similarly, an average kinetics of cooling charge in confined water HTF volumes can be deduced
 565 from the energy equation (10) and expressed as follows:

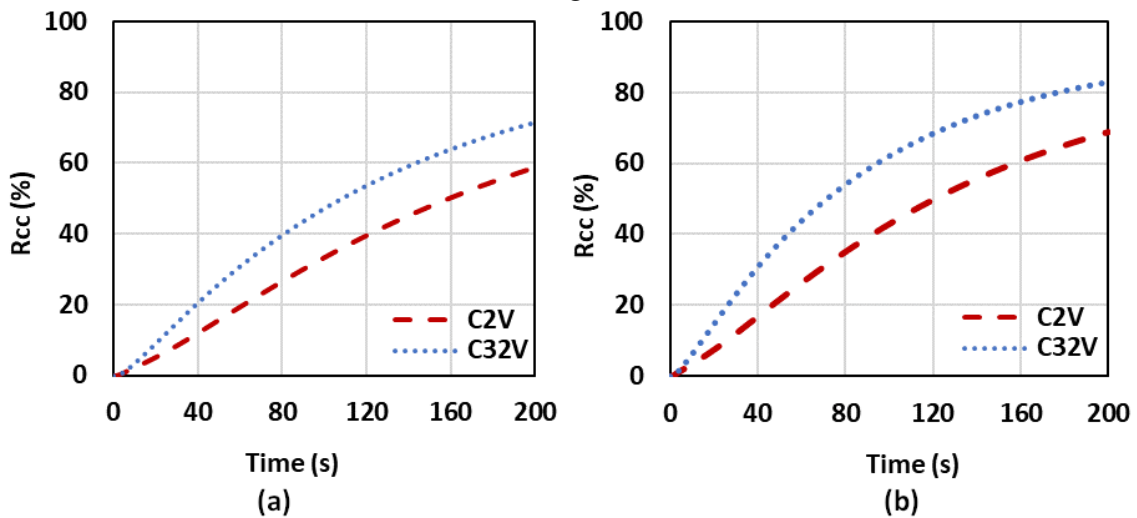
$$566 \quad \dot{T}_{cc,w} = -\frac{1}{V_w} \int \left(\frac{\lambda_w}{\rho_w C_{p,w}} \nabla^2 T \right) dV \quad (14)$$

567 Figure 13 shows the temporal evolution of the cooling charge ratio. The analysis of figure 13a
 568 shows that the cooling charge ratio in the confined water HTF volumes increases over time.
 569 This rate is higher for C32V configuration compared to C2V configuration. For example, for
 570 the lowest value of mean inlet velocity $U_{w,in} = 0.21$ m.s⁻¹, times needed to reach a cooling charge

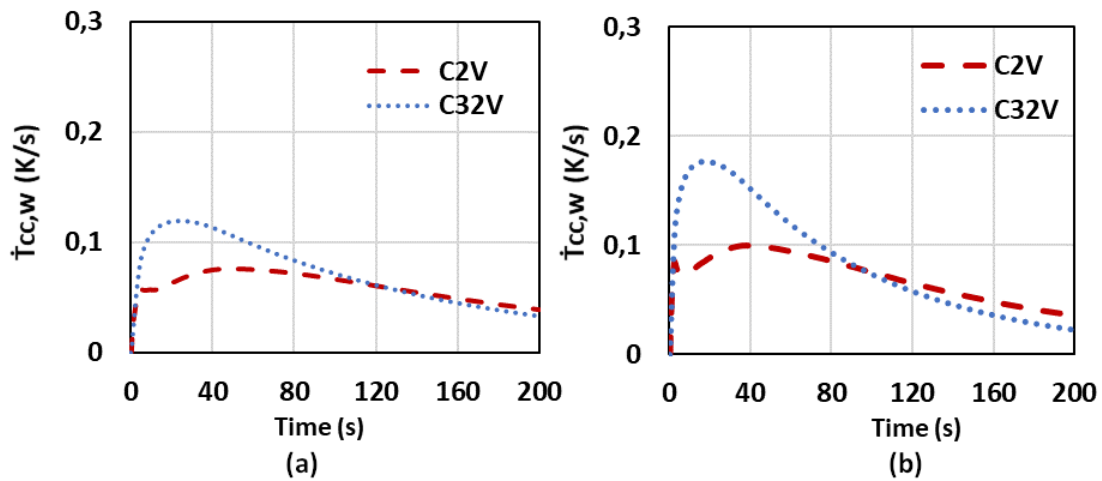
571 ratio of 60 % are approximatively 140s and 200s respectively for the C32V and C2V HTIHE
 572 geometries indicating lower charging kinetics for the HTIHE configuration C2V compared to
 573 the C32V configuration. The results are in agreement with figure 14a showing the temporal
 574 evolution of average kinetics of the cooling charge in the confined water volumes, indicating
 575 that the average kinetics is faster for the C32V configuration than the C2V configuration. In
 576 fact, by dividing the confined water HTF volumes, the conductive path in the confined water
 577 HTF becomes shorter and thus the conductive resistance smaller for the C32V configuration.
 578 On the other hand, the convective phenomena is more important for the C2V configuration with
 579 larger volumes of water.

580 It can also be noted that the kinetics of charge reaches a peak value for C32V and C2V
 581 configurations at the beginning of the charge where the temperature gradient is high. This peak
 582 value is higher for the C32V configuration compared to C2V configuration. Values are about
 583 0.12 K/s for the C32V HTIHE exchanger and about 0.08 K/s for the C2V HTIHE exchanger
 584 for $U_{w,in} = 0.21 \text{ m.s}^{-1}$ in the cooling coil (fig 14a). Over time, the temperature gradient
 585 decreases, which explains the decrease in the average kinetics of the cooling charge until
 586 reaching values close to zero for infinite charging times.

587 The same conclusions as for the first case of charging phase can be drawn from figures 13b and
 588 14b, indicating that the average kinetics of cooling charge in the confined water HTF volumes
 589 is faster for the C32V configuration than that of the C2V configuration and the cooling charge
 590 ratio in the confined water HTF volumes is higher for the C32V configuration than the C2V
 591 configuration. Furthermore, increasing the mean inlet velocity and therefore the Reynolds
 592 number in the cooling coil results in faster charge kinetics and higher ratio of cooling charge in
 593 the confined water HTF volumes for both configurations.



594
 595 *Figure 13: Temporal evolution of cooling charge ratio in the confined water HTF volumes for*
 596 *$U_{w,in} = 0.21 \text{ m.s}^{-1}$ (a) and $U_{w,in} = 0.41 \text{ m.s}^{-1}$ (b) in the cooling coil*



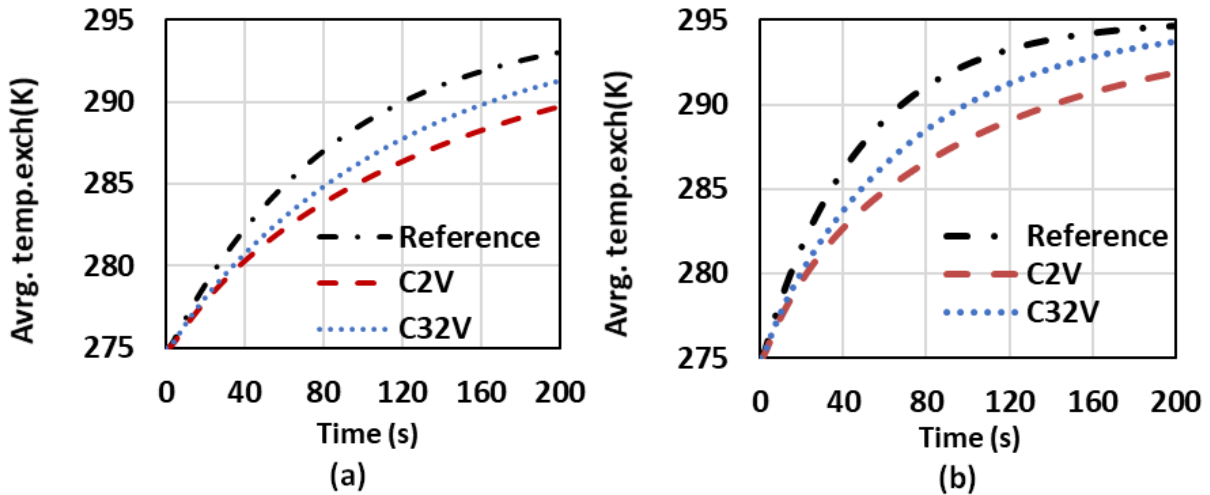
597
 598 *Figure 14: Temporal evolution of average kinetics of charging of the cold in the confined water HTF*
 599 *volumes for $U_{w,in} = 0.21 \text{ m.s}^{-1}$ (a) and $U_{w,in} = 0.41 \text{ m.s}^{-1}$ (b) in the cooling coil*

600 In order to analyze effects of the redistribution of water volumes on the thermal resistance of
 601 C2V and C32V configurations, the heat transfer exchanged at all aluminum/confined water
 602 interfaces was computed at different times for an inlet velocity $U_{w,in} = 0.21 \text{ m.s}^{-1}$ in the cooling
 603 coil. This study showed that the heat transferred was at each time significantly higher for C32V
 604 compared to C2V. The values of the heat transfer exchanged were respectively equal to 95.88,
 605 60.27 and 38.09 W for the C32V configuration at 60, 120 and 180 s, whereas they were
 606 respectively equal to 40.42, 36.57 and 27.20 W for the C2V configuration at 60, 120 and 180
 607 s. Indeed, the cold induced by the cooling heat transfer fluid is better transferred by conduction
 608 and natural convection to the entire volume of C32V configuration indicating a lower thermal
 609 resistance for C32V configuration compared to C2V configuration.

610

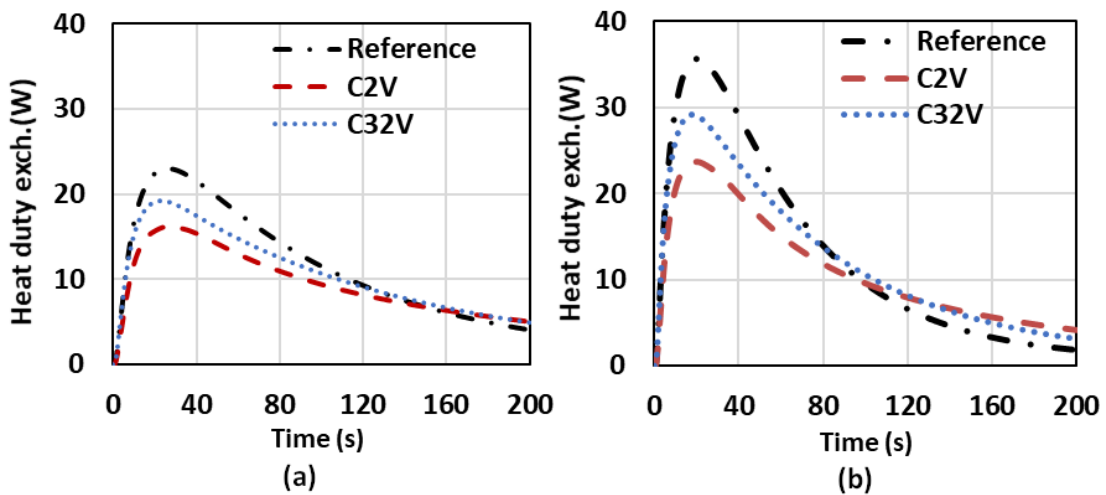
611 **4.3.2. Discharging phase of the cold**

612 The discharging time is also an important parameter to be taken into consideration in the above
 613 application. The heat exchanger has to deliver a maximum cold during the discharging period.
 614 Figure 15 shows the temporal evolution of the average heat exchangers temperature for the
 615 three configurations during the first 200 seconds of discharge respectively for mean inlet
 616 velocities values of $U_{w,in} = 0.21$ and 0.41 m.s^{-1} in the heating coil. These mean velocities
 617 correspond respectively to Reynolds numbers of about $Re_{dcoil,in} = 1000$ and 2000 . The cooling
 618 fluid is therefore stagnant in the cooling coil.



619
620 *Figure 15 : Temporal evolution of the average temperature of the exchanger for $U_{w,in} = 0.21 \text{ m.s}^{-1}$ (a)*
621 *and $U_{w,in} = 0.41 \text{ m.s}^{-1}$ (b) in the heating coil*

622 Similar to the charging phase, figure 15b shows that for the highest value of mean inlet velocity
623 $U_{w,in} = 0.41 \text{ m.s}^{-1}$, the time needed to reach a temperature level of 290 K is 65s, 98s and 140s
624 respectively for the reference, C32V and C2V HTIHE geometries indicating slightly lower
625 discharging kinetics for configurations C32V and C2V than the reference case. The same
626 conclusion is made for the lowest value of mean inlet velocity $U_{w,in} = 0.21 \text{ m.s}^{-1}$ (see figure
627 15a). This trend is clearly due to the high overall diffusivity of the reference geometry compared
628 to the innovative ones. Nevertheless, it is worth to mention that, despite 41.3% aluminium
629 substitution with stagnant low conductivity water HTF corresponding to 28.6% increase of the
630 energy density in C2V and C32V configurations, the redistribution of the confined water HTF
631 into small volumes embedded in the aluminium bloc leads to a significant increase of the
632 heating kinetics in the C32V configuration compared to the C2V configuration.



633
634 *Figure 16 : Temporal evolution of the heat transfer exchanged with the stagnant cooling fluid in the*
635 *coil for $U_{w,in} = 0.21 \text{ m.s}^{-1}$ (a) and $U_{w,in} = 0.41 \text{ m.s}^{-1}$ (b) in the heating coil*

636 Figure 16 shows the temporal evolution of heat duty exchanged with the stagnant cooling fluid
637 in the coil for mean inlet velocities values of $U_{w,in} = 0.21$ and 0.41 m.s^{-1} in the heating coil (the
638 cooling fluid does not flow during the discharging phase of cold). The results are in agreement
639 with the above discussion from figure 15 showing the temporal evolution of the average heat
640 exchangers temperature. Indeed, the heat duty exchanged with the stagnant cooling fluid
641 exhibits during the first instants of time a peak value, higher for the reference heat exchanger
642 followed by C32V and then C2V. The trend is reversed from around $t=160 \text{ s}$ for $U_{w,in} = 0.21$

643 $\text{m}\cdot\text{s}^{-1}$ (figure 16a) and $t=100$ s for $U_{w,\text{in}} = 0.41$ $\text{m}\cdot\text{s}^{-1}$ (figure 16b), and the heat duty exchanged
 644 with the stagnant cooling fluid is higher for configurations C32V and C2V compared to the
 645 reference. This is mainly due to the fact that configurations C2V and C32V have an overall
 646 higher energy density than the reference. Furthermore, more homogeneous spatial distribution
 647 of confined water HTF volumes makes heat transfer faster in the C32V configuration than in
 648 the C2V configuration.

649 A more detailed analysis of heat transfer is carried out in confined water HTF volumes during
 650 the discharge phase for configurations C2V and C32V. The maximum energy that can be
 651 released by confined water HTF volumes can be calculated from the change in the enthalpy
 652 when heating the confined water HTF from the initial temperature $T_w(t_0)$ (275 K at initial
 653 discharging time $t_0=0\text{s}$) to the final temperature $T_w(t_f)$ (295 K at the final time $t_f = \infty$) from the
 654 following equation:

$$655 \quad E_{\text{tot},w} = \rho_w C_{p,w} V_w [T_w(t_f) - T_w(t_0)] \quad (15)$$

656 Similarly, the volumetric power locally released from by each cell of the confined water HTF
 657 volumes can be deduced from the energy equation as follows:

$$658 \quad \underbrace{\rho_w C_{p,w} \frac{\partial T}{\partial t}}_{\text{Release-term}} = \underbrace{\lambda_w \nabla^2 T}_{\text{Conduction-term}} - \underbrace{\rho_w C_{p,w} \vec{V} \cdot \nabla T}_{\text{Convection-term}} \quad (16)$$

659 The cooling power released by the confined water HTF contained in these volumes can be
 660 evaluated by integrating the release term of the above equation into the total volume of confined
 661 water HTF as follows:

$$662 \quad P_{\text{vol},w} = \int \rho_w C_{p,w} \frac{\partial T}{\partial t} dV \quad (17)$$

663 The cooling energy discharged by confined water volumes can be deduced from the cooling
 664 power released by simple temporal integration between the initial discharging time $t_0 = 0\text{s}$ and
 665 any time t as follows:

$$666 \quad E_{\text{cdw}} = \int_{t_0}^t P_{\text{vol},w} dt \quad (18)$$

667 A cooling discharge ratio in the volumes of confined water HTF can be defined as follows:

$$668 \quad R_{\text{cd}} = \frac{E_{\text{cdw}}}{E_{\text{tot},w}} \cdot 100 \quad (19)$$

669 Similarly, an average kinetics of cooling discharge in confined water HTF volumes can be
 670 deduced from the energy equation (16) and expressed as follows:

$$671 \quad \dot{T}_{\text{cd},w} = \frac{1}{V_w} \int \left(\frac{\lambda_w}{\rho_w C_{p,w}} \nabla^2 T \right) dV \quad (20)$$

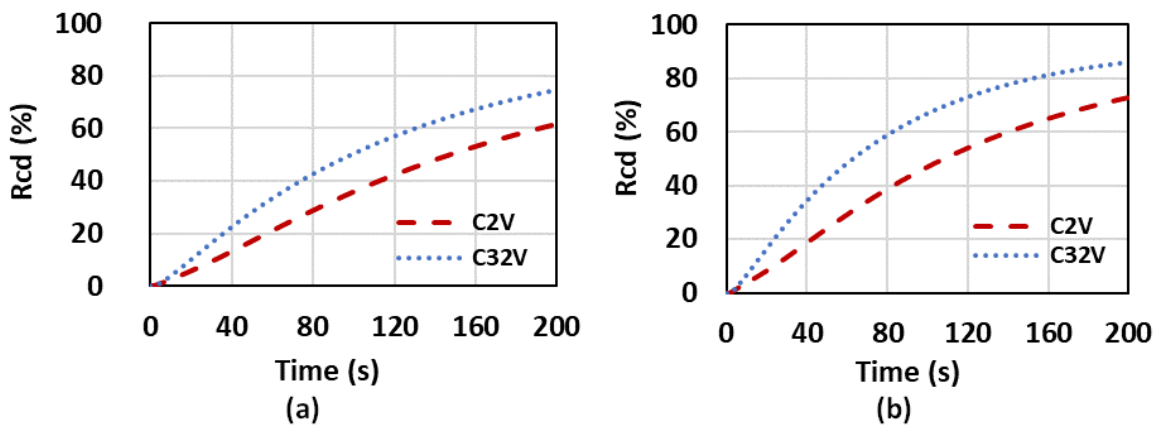
672 Figure 17 shows the temporal evolution of cooling discharge ratio. The analysis of figure 17a
 673 shows that the cooling discharge ratio in confined water volumes increases over time. This rate
 674 is higher for C32V configuration compared to C2V configuration. The results are in agreement
 675 with figure 18a showing the temporal evolution of the average kinetics of cooling discharge in
 676 confined water HTF volumes, indicating that the average kinetics is faster for the C32V
 677 configuration than the C2V configuration. Indeed, by dividing the confined water HTF
 678 volumes, the conductive path becomes shorter and thus the conductive resistance smaller for

679 the C32V configuration. On the other hand, the convective phenomena is more important for
 680 the C2V configuration with larger volumes of confined water HTF.

681 It can also be noted that the kinetics of discharge reaches a peak value for the C2V and the
 682 C32V at the beginning of the discharge where the temperature gradient is high. This peak value
 683 is higher for the C32V configuration compared to the C2V configuration. Values are about 0.12
 684 K/s for the C32V exchanger and about 0.08 K/s for the C2V HTIHE exchanger for $U_{w,in} = 0.21$
 685 $m \cdot s^{-1}$ in the heating fluid. Over time, the temperature gradient decreases, which explains the
 686 decrease in average kinetics of cooling discharge until reaching values close to zero for infinite
 687 discharging times.

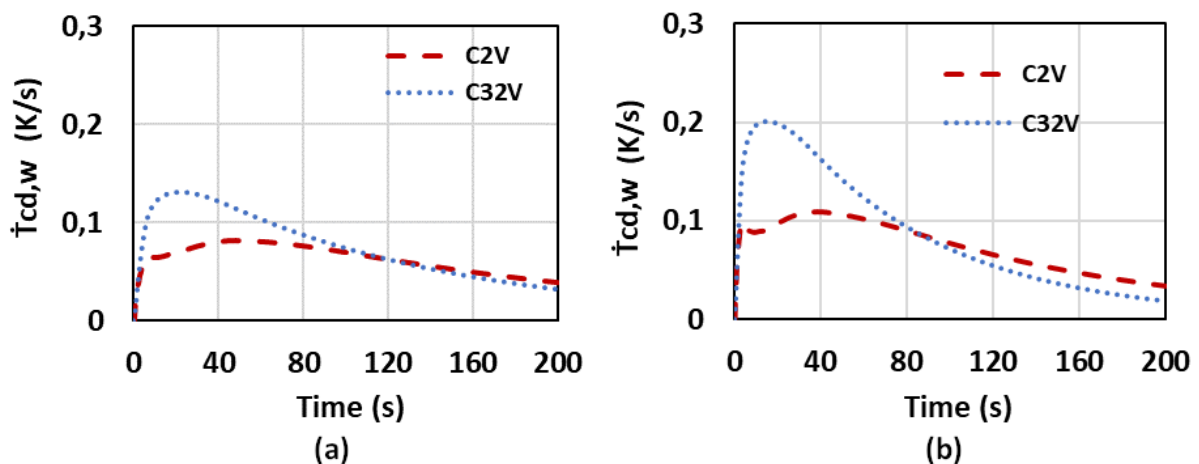
688 Similar conclusions as the first case of discharging phase can be drawn from figures 17b and
 689 18b, indicating that the average kinetics of cooling discharge in confined water HTF volumes
 690 is faster for the C32V configuration than the C2V configuration and the cooling discharge ratio
 691 in the confined water HTF volumes is higher for the C32V configuration than the C2V
 692 configuration. Furthermore, increasing the mean inlet velocity and therefore the Reynolds
 693 number of the heating fluid results in faster discharge kinetics and higher ratio of cooling
 694 discharge in the confined water HTF volumes for both configurations.

695



696

697 *Figure 17 : Temporal evolution of cooling discharge rate in confined water HTF volumes for*
 698 *$U_{w,in} = 0.21 m \cdot s^{-1}$ (a) and $U_{w,in} = 0.41 m \cdot s^{-1}$ (b) in the heating coil*



699

700 *Figure 18 : Temporal evolution of average kinetics of cooling discharge in confined water HTF*
 701 *volumes for $U_{w,in} = 0.21 m \cdot s^{-1}$ (a) and $U_{w,in} = 0.41 m \cdot s^{-1}$ (b) in the heating coil*

702

703 **5. Conclusions**

704 The design optimization of the High Thermal Inertia Heat Exchanger (HTIHE) in the food
705 industry is a very important element to improve the performance of food fluid conditioning
706 processes. A precise analysis of heat transfers in complex geometry of heat exchangers with
707 high inertia combining solid and liquid parts offer innovative solutions more efficient with
708 metallic material saving and energy performance increased. In this study, a transient numerical
709 analysis of the thermal behavior of three exchangers including a reference case having a solid
710 conductive element, and two cases derived from the reference case by a controlled substitution
711 and redistribution of 41.3% of the conductive material by a confined heat transfer fluid, was
712 performed to characterize their performance in terms of kinetics of cooling charge/discharge.
713 From this study the main conclusions are the following:

- 714 • A controlled substitution of 41.3% of conductive material, keeping constant the volume
715 of the exchanger, led to material saving compared to the reference case as well as an
716 increase the energy density of the heat exchanger by nearly 30%.
- 717 • Performances obtained with the HTIHE configurations C2V and C32V are better after
718 a certain duration of charge/discharge with, in particular, a heat duty exchanged more
719 important.
- 720 • The redistribution of the confined heat transfer fluid volumes into the overall volume of
721 the conductive material led to an increase of the heat transfer and the kinetics of
722 charge/discharge. The local geometry of the confined heat transfer fluid zones has a
723 significant influence on the performances and an optimization of the geometry of these
724 zones can allow thermal performance improvement.
- 725 • The use of a combination of fluid and solid zones inside the storage system is an
726 interesting solution allowing an increase of the storage performance with a significant
727 material reduction. The mass reduction resulting from material saving leads to easy
728 handling of the HTIHE for agro-food utilization.

729 This first study shows that it is possible to significantly improve the storage and heat transfer
730 performance of a High Thermal Inertia Heat Exchanger (HTIHE) in the food industry by
731 combining liquid and solid materials in complex geometric configurations. Future studies will
732 use temporally variable conditions (temperature and velocity) at the entries of the heating and
733 the cooling coils in order to simulate different cyclic charge-discharge scenarios and ultimately
734 consider the phase change in confined HTF volumes to benefit from the high latent heat of
735 water.

736

737 **Acknowledgements**

738 This study was carried out with the financial support of the Mines Telecom Lille Douai Institute
739 (IMT Lille Douai), the School of Advanced Engineering Studies (HEI-Yncrea-Hauts-de-
740 France) and the Hauts-de-France region via the FEDER-ESF Nord-Pas-de-Calais 2014-2020
741 program to whom we express our sincere thanks.

742

743 **References**

744 [1]X. Zhang, Q. Xue, H. Zou, J. Liu, C. Tian, X. Zhang, Influence of Heat Exchanger Tube
745 Layout on Performance of Heat Pump System for Electric Cars, Energy Procedia, Volume 105,
746 May 2017, Pages 5085-5090.

747 [2]J. Chen, Y. Liu, X. Lu, X. Ji, C. Wang, Designing heat exchanger for enhancing heat transfer
748 of slurries in biogas plants, Energy Procedia, Volume 158, February 2019, Pages 1288-1293.

- 749 [3]J. Knissel, D. Peußner, Energy efficient heat exchanger for ventilation systems, *Energy and*
750 *Buildings*, Volume 159, 15 January 2018, Pages 246-253.
- 751 [4]J. V. Simo Tala, Analysis of the flow and heat transfer characteristics in an innovative inertial
752 heat exchanger: Application to thermal energy storage, *Phys. and Chem. Phenomena in Heat*
753 *Exchangers and Multifunctional Reactors for Sustainable Technology*, Eurotherm Seminar 106,
754 10-11 Oct 2016 Paris.
- 755 [5]C. R. Chandra Rao, H. Niyas, P. Muthukumar, Performance tests on lab-scale sensible heat
756 storage prototypes, *Applied Thermal Engineering*, Volume 129, 25 January 2018, Pages 953-
757 967.
- 758 [6]D. Lafri, D. Semmar, A. Hamid, M. Ouzzane, Experimental investigation on combined
759 sensible and latent heat storage in two different configurations of tank filled with PCM, *Applied*
760 *Thermal Engineering*, Volume 149, 25 February 2019, Pages 625-632.
- 761 [7]Chandrashekara, M., A. Yadav, An experimental study of the effect of exfoliated graphite
762 solar coating with a sensible heat storage and Scheffler dish for desalination, *Applied Thermal*
763 *Engineering*, Volume 123, August 2017, Pages 111-122.
- 764 [8]L. Geissbühler, M. Kolman, G. Zanganeh, A. Haselbacher, A. Steinfeld, Analysis of
765 industrial-scale high-temperature combined sensible/latent thermal energy storage, *Applied*
766 *Thermal Engineering*, Volume 101, 25 May 2016, Pages 657-668.
- 767 [9]K.A.R. Ismaila, R. Stuginsky Jra, A parametric study on possible fixed bed models for pcm
768 and sensible heat storage, *Applied Thermal Engineering*, Volume 19, Issue 7, July 1999, Pages
769 757-788.
- 770 [10]S. Kunkel, T. Teumer, P. Dörnhofer, K. Schlachter, Y. Weldeleslasie, M. Kühr, M. Rädle,
771 J. Repke, Determination of heat transfer coefficients in direct contact latent heat storage
772 systems, *Applied Thermal Engineering*, Volume 145, 25 December 2018, Pages 71-79.
- 773 [11]D. Maderić, B. Pavković, K. Lenić, An experimental research on energy efficiency of a
774 beverage cooler with the latent heat storage, *Applied Thermal Engineering*, Volume 148, 5
775 February 2019, Pages 270-277.
- 776 [12]R. Abdulrahman, F. Ibrahim, S. Dakhil, Development of paraffin wax as phase change
777 material based latent heat storage in heat exchanger, *Applied Thermal Engineering*, Volume
778 150, 5 March 2019, Pages 193-199.
- 779 [13]M. Kabbara, D. Groulx, A. Joseph, Experimental investigations of a latent heat energy
780 storage unit using finned tubes, *Applied Thermal Engineering*, Volume 101, 25 May 2016,
781 Pages 601-611.
- 782 [14]M. Kubota, S. Matsumoto, H. Matsuda, Enhancement of hydration rate of LiOH by
783 combining with mesoporous carbon for Low-temperature chemical heat storage, *Applied*
784 *Thermal Engineering*, Volume 150, 5 March 2019, Pages 858-863.
- 785 [15]O. Myagmarjav, M. Zamengo, J. Ryu, Y. Kato, Energy density enhancement of chemical
786 heat storage material for magnesium oxide/water chemical heat pump, *Applied Thermal*
787 *Engineering*, Volume 91, 5 December 2015, Pages 377-386.
- 788 [16]O. Myagmarjav, J. Ryu, Y. Kato, Lithium bromide-mediated reaction performance
789 enhancement of a chemical heat-storage material for magnesium oxide/water chemical heat
790 pumps, *Applied Thermal Engineering*, Volume 63, Issue 1, 5 February 2014, Pages 170-176.
- 791 [17]H. Singh, R.P. Saini, J.S. Saini, A review on packed bed solar energy storage systems,
792 *Renewable and Sustainable Energy Reviews*, Volume 14, Issue 3, April 2010, Pages 1059-
793 1069.
- 794 [18]A. Kumar and S.K. Shukla, A Review on Thermal Energy Storage Unit for Solar Thermal
795 Power Plant Application, *Energy Procedia*, Volume 74, August 2015, Pages 462-469.

- 796 [19]A. Dinker, M. Agarwal, G.D. Agarwal, Heat storage materials, geometry and applications:
797 A review, *Journal of the Energy Institute*, Volume 90, Issue 1, February 2017, Pages 1-11.
- 798 [20]J. Xu, R.Z. Wang, Y. Li, A review of available technologies for seasonal thermal energy
799 storage, *Solar Energy*, Volume 103, May 2014, Pages 610-638.
- 800 [21]G. Li, Sensible heat thermal storage energy and exergy performance evaluations,
801 *Renewable and Sustainable Energy Reviews*, Volume 53, January 2016, Pages 897-923.
- 802 [22]A.I. Fernandez, M. Martínez, M. Segarra, I. Martorell, L. F. Cabeza, Selection of materials
803 with potential in sensible thermal energy storage, *Solar Energy Materials and Solar Cells*,
804 Volume 94, Issue 10, October 2010, Pages 1723-1729.
- 805 [23]L. F. Cabeza, E. Galindo, C. Prieto, C. Barreneche, A. Inés Fernández, Key performance
806 indicators in thermal energy storage: Survey and assessment, *Renewable Energy*, Volume 83,
807 November 2015, Pages 820-827.
- 808 [24]A. Gil, M. Medrano, I. Martorell, A. Lázaro, P. Dolado, B. Zalba, L.F. Cabeza, State of the
809 art on high temperature thermal energy storage for power generation. Part 1-Concepts, materials
810 and modellization, *Renewable and Sustainable Energy Reviews*, Volume 14, Issue 1, January
811 2010, Pages 31-55.
- 812 [25]S. Khare, M. Dell'Amico, C. Knight, S. McGarry, Selection of materials for high
813 temperature sensible energy storage, *Solar Energy Materials and Solar Cells*, Volume
814 115, August 2013, Pages 114-122.
- 815 [26]O. Ercan Ataer, Storage Of Thermal Energy, in *Energy Storage Systems*, in *Encyclopedia*
816 *of Life Support Systems (EOLSS)*, Developed under the Auspices of the UNESCO, Eolss
817 Publishers, Oxford, UK, 2006.
- 818 [27]S. M. Hasnain, Review on sustainable thermal energy storage technologies, Part I: heat
819 storage materials and techniques, *Energy Conversion and Management*, Volume 39, Issue 11,
820 1 August 1998, Pages 1127-1138.
- 821 [28]E.M. Alawadhi, Thermal analysis of a building brick containing phase change material,
822 *Energy and Buildings*, Volume 40, Issue 3, 2008, Pages 351-357.
- 823 [29]E. Özrahat, S. Ünalán, Thermal performance of a concrete column as a sensible thermal
824 energy storage medium and a heater, *Renewable Energy*, Volume 111, October 2017, Pages
825 561-579.
- 826 [30]R. Tiskatine, R. Oaddi, R. Ait El Cadi, A. Bazgaou, L. Bouirden, A. Aharoune, A. Ihlal,
827 Suitability and characteristics of rocks for sensible heat storage in CSP plants, *Solar Energy*
828 *Materials and Solar Cells*, Volume 169, September 2017, Pages 245-257.
- 829 [31]D. Laing, W. Steinmann, R. Tamme, C. Richter, Solid media thermal storage for parabolic
830 trough power plants, *Solar Energy*, Volume 80, Issue 10, October 2006, Pages 1283-1289.
- 831 [32]L. Prasad, P. Muthukumar, Design and optimization of lab-scale sensible heat storage
832 prototype for solar thermal power plant application, *Solar Energy*, Volume 97, November 2013,
833 Pages 217-229.
- 834 [33]M. K. A. Sharif, A. A. AlAbidi, S. Mat, K. Sopian, M. H. Ruslan, M.Y. Sulaiman, M. A.
835 M. Rosli, Review of the application of phase change material for heating and domestic hot
836 water systems, *Renewable and Sustainable Energy Reviews*, Volume 42, February 2015, Pages
837 557-568.
- 838 [34]Z. Yang, S. V. Garimella, Thermal analysis of solar thermal energy storage in a molten-salt
839 thermocline, *Solar Energy*, Volume 84, Issue 6, June 2010, Pages 974-985.
- 840 [35]L. EL-Kaddadi, M. Asbik, N. Zari, B. Zeghmati, Experimental study of the sensible heat
841 storage in the water/TiO₂ nanofluid enclosed in an annular space, *Applied Thermal*
842 *Engineering*, Volume 122, 25 July 2017, Pages 673-684.

- 843 [36]H.E. Thomason, Solar space heating and air conditioning in the Thomason Home, Solar
844 Energy, Volume 4, Issue 4, October 1960, Pages 11-19.
- 845 [37]A.E. Moschatos, Combined thermal storage, Solar Energy, Volume 51, Issue 5, 1993, Pages
846 391-399.
- 847 [38]R. Lugolole, A.Mawire, K. A. Lentswe, D. Okello, K. Nyeinga, Thermal performance
848 comparison of three sensible heat thermal energy storage systems during charging cycles,
849 Sustainable Energy Technologies and Assessments, Volume 30, December 2018, Pages 37-51.
- 850 [39]J. S. Jayakumar, S. M. Mahajania, J. C. Mandala, Kannan N. Iyer, P. K. Vijayan, CFD
851 analysis of single-phase flows inside helically coiled tubes, Computers & Chemical
852 Engineering, Volume 34, Issue 4, 5 April 2010, Pages 430-446.
- 853 [40]J. S. Jayakumar, S.M. Mahajani, J. C. Mandal, P. K. Vijayan, R. Bhoi, Experimental and
854 CFD estimation of heat transfer in helically coiled heat exchangers, Chemical Engineering
855 Research and Design, Volume 86, Issue 3, March 2008, Pages 221-232.
- 856 [41]CD-Adapco. Starccm+ v10 user guide. User guide, 2017.
- 857 [42]G. de Vahl Davis, I. P. Jones, Natural Convection of Air in a Square Cavity: A comparison
858 Exercise, International Journal for Numerical Methods in Fluids, volume 3, pp. 227-248, 1983.
- 859 [43]M. Ghobadi, Y. S. Muzychka, A review of heat transfer and pressure drop correlations for
860 laminar flow in curved circular ducts, Heat Transfer Engineering, Volume 37, Issue 10, 2015.